NASA TECHNICAL NOTE

NASA TN D-5978

NASA TN D-5978

REFLECTION COEFFICIENTS OF PYRAMIDAL AND H-PLANE HORNS RADIATING INTO DIELECTRIC MATERIALS

by C. R. Cockrell

Langley Research Center
Hampton, Va. 23365

NATIONAL AERONAUTICS AND SPACE ADMINISTRATION • WASHINGTON, D. C. • SEPTEMBER 1970

1. Report No.	2. Government Accession No.	3. Recipient's Catalog No.
NASA TN D-5978		

4. Title and Subtitle
REFLECTION COEFFICIENTS OF PYRAMIDAL AND H-PLANE HORNS RADIATING INTO DIELECTRIC MATERIALS

5. Report Date
September 1970

6. Performing Organization Code

7. Author(s)
C. R. Cockrell

8. Performing Organization Report No.
L-7203

10. Work Unit No.
125-21-04-06

9. Performing Organization Name and Address
NASA Langley Research Center
Hampton, Va. 23365

11. Contract or Grant No.

13. Type of Report and Period Covered
Technical Note

12. Sponsoring Agency Name and Address
National Aeronautics and Space Administration
Washington, D.C. 20546

14. Sponsoring Agency Code

15. Supplementary Notes The information presented herein was included in a thesis entitled "Reflection Coefficients of Horns Radiating Into Dielectric Materials" offered in partial fulfillment of the requirements for the degree of Master of Science in Electrical Engineering, George Washington University, Washington, D.C., February 1970.

16. Abstract

The admittance of a uniform rectangular waveguide-fed aperture is assumed to approximate the mouth admittances of the pyramidal and H-plane horns. Calculations of the admittances (or reflection coefficients) were obtained for the rectangular-mouth sizes of the pyramidal and H-plane horns under free-space conditions and with the horns radiating into slabs of plexiglass or quartz. Measurements were obtained for a number of slab thicknesses.

Good agreement was obtained between the measured and calculated reflection coefficients for the pyramidal horn; agreement for the H-plane horns was not as good. The reflection coefficients measured for an H-plane horn with a 9^{o} flare angle more closely approximated the calculated values than did the measured values for an 18^{o} flare angle, particularly in magnitude.

The results of the present study indicate that the expressions for the admittance of a uniform rectangular waveguide-fed aperture can be used to approximate the mouth admittances of the pyramidal and H-plane horn. The accuracy of this approximation is similar to that obtained with rectangular waveguides opening onto small ground planes covered with slabs of material.

The admittance of a uniform rectangular waveguide-fed aperture has been shown to approach the admittance of a parallel-plate waveguide radiating into a slab of homogeneous material as the long dimension of the aperture becomes infinite. This result has been shown both analytically and numerically (for free-space conditions) for the dominant mode.

17. Key Words (Suggested by Author(s))	18. Distribution Statement
Reflection coefficients Horns Dielectric materials	Unclassified – Unlimited

19. Security Classif. (of this report)	20. Security Classif. (of this page)	21. No. of Pages	22. Price*
Unclassified	Unclassified	49	$3.00

*For sale by the Clearinghouse for Federal Scientific and Technical Information
Springfield, Virginia 22151

REFLECTION COEFFICIENTS OF PYRAMIDAL AND H-PLANE HORNS RADIATING INTO DIELECTRIC MATERIALS*

By C. R. Cockrell
Langley Research Center

SUMMARY

The admittance of a uniform rectangular waveguide-fed aperture is assumed to approximate the mouth admittances of the pyramidal and H-plane horns. Calculations of the admittances (or reflection coefficients) were obtained for the rectangular-mouth sizes of the pyramidal and H-plane horns under free-space conditions and with the horns radiating into slabs of plexiglass or quartz. Measurements were obtained for a number of slab thicknesses.

Good agreement was obtained between the measured and calculated reflection coefficients for the pyramidal horn; agreement for the H-plane horns was not as good. The reflection coefficients measured for an H-plane horn with a 9^{o} flare angle more closely approximated the calculated values than did the measured values for an 18^{o} flare angle, particularly in magnitude.

The results of the present study indicate that the expressions for the admittance of a uniform rectangular waveguide-fed aperture can be used to approximate the mouth admittances of the pyramidal and H-plane horn. The accuracy of this approximation is similar to that obtained with rectangular waveguides opening onto small ground planes covered with slabs of material.

The admittance of a uniform rectangular waveguide-fed aperture has been shown to approach the admittance of a parallel-plate waveguide radiating into a slab of homogeneous material as the long dimension of the aperture becomes infinite. This result has been shown both analytically and numerically (for free-space conditions) for the dominant mode.

---

*The information presented herein was included in a thesis entitled "Reflection Coefficients of Horns Radiating Into Dielectric Materials" offered in partial fulfillment of the requirements for the degree of Master of Science in Electrical Engineering, George Washington University, Washington, D.C., February 1970.

INTRODUCTION

The electromagnetic horn is used quite extensively in spacecraft applications for pattern considerations and plasma diagnostics. Often, horn antennas are mounted on the metallic body of a spacecraft in such a manner that the horn mouth is flush with the body. Generally, the spacecraft is covered with thick layers of dielectric ablative material for protecting the internal instrumentation from the intense heat during hypersonic reentry into the earth's atmosphere. This intense heat will cause the properties of the dielectric material to change; and as a result, the admittance characteristics of the horn antenna will also change.

The mouth admittances of horns have not been successfully treated theoretically. Experimentally, the mouth admittances of horns are determined from measurements in the feeding uniform waveguide. (See refs. 1 and 2.) Equations describing the wave admittance in the sectoral horn are given by Risser (ref. 1) and Wolff (ref. 2). These equations can be used to determine the reflection coefficient at any point in the sectoral horn if the admittance is known at that point.

The purpose of this paper is to determine an approximate expression for the mouth admittances of the pyramidal horn and the H-plane sectoral horn radiating into slabs of homogeneous dielectric material. The mouth admittance of the pyramidal horn is assumed to be approximated by the admittance of a uniform rectangular waveguide-fed aperture. The mouth admittance of the H-plane horn is shown to be approximated by the same expression.

Variational expressions for the admittance of a uniform rectangular waveguide-fed aperture covered with slabs of homogeneous material have been derived in references 3 to 5. In papers by Galejs (refs. 6 to 8), a trial field in the aperture was assumed to be a superposition of a sine wave and a shifted cosine wave. This solution is also variational, but the infinite ground-plane structure was approximated by a large waveguide. Many authors have assumed only the TE_{01} mode as a trial field at the aperture which is terminated in an infinite ground plane. The possibilities of contributions of a higher order, odd symmetrical mode (the TE_{03} mode) to the aperture admittance have also been investigated. (See refs. 9 and 10.) If the admittance of a uniform rectangular waveguide-fed aperture can be assumed to approximate the mouth admittance of a horn, a technique can be developed for determining the properties of the dielectric material covering the horn. Hence, either the pyramidal or the H-plane horn can be used as a diagnostic tool for making parametric studies.

The mouth admittances of two H-plane sectoral horns and one pyramidal horn are investigated with and without a low-loss dielectric material covering a ground plane. Two H-plane sectoral horns with different flare angles (9° and 18°) and a fixed mouth size

were chosen to demonstrate how the theoretical computations can better approximate the measured admittance values (or reflection coefficients) if the flare angle is decreased.

In the appendix, the admittance of the rectangular aperture is shown to approach the admittance of a parallel-plate waveguide radiating into a slab of homogeneous material as the long dimension of the rectangular aperture becomes infinite. This result is shown both analytically and numerically (for free-space conditions).

SYMBOLS

a short dimension of waveguide

b long dimension of waveguide

$C_0(k_x), C_1(k_y)$ functions defined by equations (A2a) and (A2b), respectively

d thickness of slab

E electric field intensity

$f(\beta,z), g(\beta,z)$ normalized Fourier transforms of vector potentials

$g_{s,n}$ surface-wave conductance where n refers to specific poles

H magnetic field intensity

$H_n^{(1)}(k,\rho)$, $H_n^{(2)}(k,\rho)$ Hankel functions of first and second kind, respectively, of order n

$j = \sqrt{-1}$

k_o wave number in free space, $\omega\sqrt{\epsilon_o \mu_o}$

k_x, k_y Cartesian components of wave number

k_z^{II} wave number in dielectric-material region

k_z^{III} wave number in free-space region

x,y,z Cartesian coordinates

Y admittance in sectoral horn

Y_{ap} aperture admittance

$Y_{ap,p}$ aperture admittance for parallel-plate waveguide

Y_c characteristic admittance of sectoral horn

Y_o characteristic admittance of free space

Y_{01}, Y_{03} characteristic admittance of TE_{01} and TE_{03} modes, respectively, in waveguide region, $Y_{01} = Y_o\sqrt{1 - \left(\frac{\pi}{k_o b}\right)^2}$, $Y_{03} = -jY_o\sqrt{\left(\frac{3\pi}{k_o b}\right)^2 - 1}$

$Y_{11} = y_{11}Y_{01}$

y_{ap} normalized aperture admittance

y_{03} normalized value of Y_{03}, $\frac{Y_{03}}{Y_{01}}$

y_{11}, y_{13}, y_{33} terms defined by equations (2a), (2b), and (2c), respectively

α,β polar component for $\frac{k_x}{k_o}$ and $\frac{k_y}{k_o}$, respectively

β_n surface-wave pole

Γ reflection coefficient in uniform waveguide

Γ_s reflection coefficient in sectoral horn

ϵ_o permittivity of free space

ϵ_1 permittivity of dielectric material

θ spherical coordinate

λ wavelength in free space

μ_0 permeability of free space

ρ,ϕ,z cylindrical coordinates

ω angular operating frequency

Superscripts:

TE transverse electric

TM transverse magnetic

Subscripts:

ρ,ϕ,z direction components of cylindrical coordinates

Primes denote derivatives.

PYRAMIDAL HORN

Design

The pyramidal horn, details of which are shown in figure 1, was designed originally for tests in an arc-jet facility at the Langley Research Center. For such tests, the throat aperture of the horn was reduced slightly from standard X-band waveguide dimensions, that is, from 1.016 by 2.286 cm to 0.953 by 1.905 cm. From the throat, the horn flares linearly in the E- and H-planes at angles of approximately 8.7° and 9.0°, respectively. The overall length is 15.240 cm. These dimensions fix the mouth size at 3.302 by 4.318 cm, with the larger dimension corresponding to the H-plane. A plate is provided at the mouth of the horn for the purpose of mounting a ground plane or of attaching the horn to a spacecraft. The throat is terminated in a flange for connecting to a waveguide. The wall thickness is approximately 0.317 cm.

Experiment

A 30.480-cm-square ground plane was attached to the plate at the mouth of the horn. A waveguide-to-waveguide adapter was connected to the throat flange. This adapter (transition) enabled the horn to be connected to a standard RG 52/U waveguide. The horn

was then connected to a microwave test setup as shown by the schematic drawing given in figure 2.

The mouth admittance of the pyramidal horn was determined over a frequency range from 10.0 to 10.6 GHz in 0.2-GHz increments. Each frequency was accurately set by the frequency meter. Measurements were made for the horn radiating into free space and into one of several plexiglass or quartz dielectric slabs. The plexiglass slabs were of eight different thicknesses: 0.154, 0.246, 0.345, 0.490, 0.574, 0.932, 0.987, and 1.241 cm. The quartz slabs were of three thicknesses: 0.322, 0.635, and 1.295 cm. To reduce any reflections that might occur from the surrounding environment, microwave-absorbent material was placed around the horn for all measurements. The magnitude and phase of the reflection coefficient for the pyramidal horn radiating into free space (d = 0 cm) and into the various slab thicknesses are shown in figure 3 for plexiglass and in figure 4 for quartz over the indicated frequency range.

Calculations

The equations for determining the admittance of a uniform rectangular waveguide-fed aperture were derived in reference 9 by using the approach of reference 11 and are given here for convenience. The aperture admittance for the dominant TE_{01} mode plus the next higher order, odd symmetrical mode (the TE_{03} mode) is given by

$$y_{ap} = y_{11} - \frac{y_{13}^2}{y_{33} + y_{03}} \tag{1}$$

where

$$y_{11} = -j \frac{2k_o^2 ab}{\frac{Y_{01}}{Y_o}} \int_{\beta=0}^{\infty} \int_{\alpha=0}^{2\pi} \left(\frac{\sin \frac{k_o \beta a \cos \alpha}{2}}{\frac{k_o \beta a \cos \alpha}{2}} \right)^2 \left[\frac{\cos \frac{k_o \beta b \sin \alpha}{2}}{\pi^2 - (k_o \beta b \sin \alpha)^2} \right]^2 \left[- \frac{g'(\beta,0)}{k_o g(\beta,0)} \sin^2 \alpha + \frac{\epsilon_1}{\epsilon_o} \frac{k_o f(\beta,0)}{f'(\beta,0)} \cos^2 \alpha \right] \beta d\beta \, d\alpha \tag{2a}$$

$$y_{13} = -j \frac{2k_o^2 ab}{\frac{Y_{01}}{Y_o}} \int_{\beta=0}^{\infty} \int_{\alpha=0}^{2\pi} \left(\frac{\sin \frac{k_o \beta a \cos \alpha}{2}}{\frac{k_o \beta a \cos \alpha}{2}} \right)^2 \left\{ \frac{-3 \cos^2 \frac{k_o \beta b \sin \alpha}{2}}{\left[\pi^2 - (k_o \beta b \sin \alpha)^2 \right] \left[(3\pi)^2 - (k_o \beta b \sin \alpha)^2 \right]} \right\} \times \left[- \frac{g'(\beta,0)}{k_o g(\beta,0)} \sin^2 \alpha + \frac{\epsilon_1}{\epsilon_o} \frac{k_o f(\beta,0)}{f'(\beta,0)} \cos^2 \alpha \right] \beta d\beta \, d\alpha \tag{2b}$$

$$y_{33} = -j\frac{2k_o^2 ab}{\frac{Y_{01}}{Y_o}}\int_{\beta=0}^{\infty}\int_{\alpha=0}^{2\pi}\left(\frac{\sin\frac{k_o\beta a\cos\alpha}{2}}{\frac{k_o\beta a\cos\alpha}{2}}\right)^2\left[\frac{3\cos\frac{k_o\beta b\sin\alpha}{2}}{(3\pi)^2-(k_o\beta b\sin\alpha)^2}\right]^2\left[-\frac{g'(\beta,0)}{k_o g(\beta,0)}\sin^2\alpha\right.$$

$$\left.+\frac{\epsilon_1}{\epsilon_o}\frac{k_o f(\beta,0)}{f'(\beta,0)}\cos^2\alpha\right]\beta\,d\beta\,d\alpha \qquad (2c)$$

$$\left.\begin{aligned} y_{03} &= \frac{Y_o}{Y_{01}}\sqrt{1-\left(\frac{3\pi}{k_o b}\right)^2} \qquad \left(\text{for } \frac{3\pi}{k_o b} < 1\right)\\ y_{03} &= -j\frac{Y_o}{Y_{01}}\sqrt{\left(\frac{3\pi}{k_o b}\right)^2-1} \qquad \left(\text{for } \frac{3\pi}{k_o b} > 1\right)\end{aligned}\right\} \qquad (2d)$$

For the mouth size of the pyramidal horn, the dimensions a and b equal 3.302 and 4.318 cm, respectively. The thickness d of the material covering the ground plane and horn mouth was varied from 0.0 to 2.0 cm in 0.1-cm increments. The complex dielectric constant ϵ_1 was assumed to be 2.55 - j0.01 for plexiglass and 3.76 - j0.01 for quartz. A small loss was assumed to alleviate the surface-wave problems that occur in the integration (see ref. 9) when the dielectric constant is lossless. The frequency range was the same as the range used in making the measurements; that is, the frequency varied from 10.0 to 10.6 GHz in 0.2-GHz increments.

Equation (1) includes the contribution of the higher order TE_{03} mode as the term $\frac{-(y_{13}^2)}{y_{33}+y_{03}}$. For the mouth size of 3.302 by 4.318 cm, the effect of this term on the admittance is negligible as shown by the calculations presented in table I for several frequencies and several thicknesses of plexiglass. Therefore, the admittance obtained by assuming only the TE_{01} mode in the aperture is sufficient. Because the flare angles of the horn are small and the wave is assumed to be a plane wave at the mouth of the horn, the reflection coefficient, both magnitude and phase, is computed from the normalized admittance by the relationship

$$\Gamma = \frac{1-y_{ap}}{1+y_{ap}} \qquad (3)$$

Measured and calculated values of the magnitude and phase of the reflection coefficient are plotted as a function of slab thickness in figure 3 for plexiglass and in figure 4 for quartz. The reflection coefficient given by equation (3) is based on the assumption that

the flare angles have little effect on the aperture admittance. The agreement between the measured and calculated data indicates that this assumption is valid.

Discussion of Results

Good general agreement was obtained between measured and calculated values of the magnitude and phase of the reflection coefficient for most of the slab samples, with better agreement being observed for the plexiglass slabs. (Compare figs. 3 and 4.) The greatest disagreement occurred in the magnitude of the reflection coefficient determined for the 0.322-cm-thick quartz slab. (See fig. 4.) Since excellent agreement was obtained for free-space conditions, the errors are caused by the slabs. The inability to clamp the samples snugly to the ground plane and the nonuniformities in the slab samples will cause some errors in the measurements. In addition to these sources of error, the finite edges of the slabs could influence the aperture admittance (or reflection coefficient) if surface waves are strongly coupled into the slabs. In the theoretical model, the dielectric constants of the slabs were assumed to have a small loss for computational reasons, that is, to eliminate the problem of computing the surface-wave conductances. In the experimental model, the finite edges of the slabs cause reflections of the surface waves which must be considered. The 30.480-cm-square slab is not lossy enough to damp out these quasi-surface waves at the finite edges of the slab. Therefore, the conductance of the aperture admittance for infinite slabs of material was investigated.

Equations for determining conductance as a result of the surface-wave poles are presented in reference 9. In the notation of the present investigation, these equations are as follows:

$$g_{s,n}^{TE} = \frac{4\pi k_o^2 ab}{\frac{Y_{01}}{Y_o}} \sum_n \frac{\left(\frac{\epsilon_1}{\epsilon_o} - \beta_n^2\right) \int_0^{\pi} \left(\frac{\sin \frac{k_o \beta_n a \cos \alpha}{2}}{\frac{k_o \beta_n a \cos \alpha}{2}} \right)^2 \left[\frac{\cos \frac{k_o \beta_n b \sin \alpha}{2}}{\pi^2 - (k_o \beta_n b \sin \alpha)^2} \right]^2 \sin^2 \alpha \, d\alpha}{k_o d \left[1 - \frac{\left(\frac{\epsilon_1}{\epsilon_o} - 1\right)}{\left(\beta_n^2 - 1\right)} \frac{\sin 2k_o d \sqrt{\frac{\epsilon_1}{\epsilon_o} - \beta_n^2}}{2k_o d \sqrt{\frac{\epsilon_1}{\epsilon_o} - \beta_n^2}} \right]} \tag{4a}$$

$$g_{s,n}^{TM} = \frac{4\pi k_o^2 ab}{\frac{Y_{01}}{Y_o}} \left[\frac{\epsilon_1}{\epsilon_o} \int_0^{\pi} \left(\frac{\sin \frac{k_o \beta_n a \cos \alpha}{2}}{\frac{k_o \beta_n a \cos \alpha}{2}} \right)^2 \left[\frac{\cos \frac{k_o \beta_n b \sin \alpha}{2}}{\pi^2 - (k_o \beta_n b \sin \alpha)^2} \right]^2 \cos^2 \alpha \, d\alpha \right]_n \Bigg/ k_o d \left[1 + \frac{\left(\frac{\epsilon_1}{\epsilon_o} - 1 \right)}{\left(\beta_n^2 - 1 \right)} \frac{\sin 2k_o d \sqrt{\frac{\epsilon_1}{\epsilon_o} - \beta_n^2}}{2k_o d \sqrt{\frac{\epsilon_1}{\epsilon_o} - \beta_n^2}} \right] \tag{4b}$$

where values of β_n are roots of the transcendental equations

$$\left.\begin{aligned} \tan k_o d \sqrt{\frac{\epsilon_1}{\epsilon_o} - \beta^2} &= -\frac{\sqrt{\frac{\epsilon_1}{\epsilon_o} - \beta^2}}{\sqrt{\beta^2 - 1}} \qquad \text{(Transverse electric)} \\ \tan k_o d \sqrt{\frac{\epsilon_1}{\epsilon_o} - \beta^2} &= \frac{\frac{\epsilon_1}{\epsilon_o} \sqrt{\beta^2 - 1}}{\sqrt{\frac{\epsilon_1}{\epsilon_o} - \beta^2}} \qquad \text{(Transverse magnetic)} \end{aligned}\right\} \tag{5}$$

The surface-wave conductance given by equations (4) and (5), the total conductance, and the percentage of surface-wave conductance contained in the total conductance are given in table II for the 0.322-cm-thick quartz slab and for the 0.345-cm-thick plexiglass slab. The percentage of surface-wave conductance is small for both slabs; however, the percentage for the quartz slab is greater. The greater the surface-wave conductance, the greater the effect the outer edge could have on the aperture admittance (or reflection coefficient). This effect could be sufficient to reduce the magnitude of the reflection coefficient and could account for some of the error in the quartz-slab data shown in figure 4. The same kind of error was observed for a standard X-band waveguide (1.016 by 2.286 cm) radiating into a dielectric slab of about the same thickness. (See ref. 12.)

To illustrate the effects the slabs have upon the antenna pattern, E-plane radiation patterns were measured at 10.0 GHz for the pyramidal horn radiating into free space, into the 0.322-cm-thick quartz slab (see fig. 5), and into the 0.345-cm-thick plexiglass slab (see fig. 6). A greater amount of ripple is observed in the pattern for the quartz slab than in the pattern for the plexiglass slab. If the amount of ripple in the pattern increases, the trapped energy increases (ref. 13), and as a result, the surface wave increases.

By fixing the H-plane mouth width as 4.318 cm and varying the E-plane mouth height, the surface-wave conductance was computed at 10.0 GHz for the two dielectric slabs. A plot of the normalized surface-wave conductance as a function of E-plane mouth height is shown in figure 7 for the 0.322-cm-thick quartz slab and the 0.345-cm-thick plexiglass slab. Similar graphs for different frequencies and slab thicknesses can be made. By choosing the proper E-plane height for the fixed H-plane width, the surface-wave conductance can be kept at a minimum. Perhaps if the pyramidal horn were designed to minimize the occurrence of surface-wave conductance, the measured and calculated reflection coefficients would be in better agreement.

H-PLANE HORNS

Design

With reference to the sketch given in figure 8, the dominant-mode fields in an H-plane sectoral horn are presented in reference 2 (p. 222) and are repeated here because the order of the Hankel functions was a design criterion:

$$\left.\begin{aligned} E_z &= A \cos n\phi\left[H_n^{(2)}(k_o\rho) + \alpha H_n^{(1)}(k_o\rho)\right] \\ H_\rho &= \frac{nA \sin n\phi}{j\omega\mu_o\rho}\left[H_n^{(2)}(k_o\rho) + \alpha H_n^{(1)}(k_o\rho)\right] \\ H_\phi &= \frac{k_o A \cos n\phi}{j\omega\mu_o}\left[H_n^{(2)'}(k_o\rho) + \alpha H_n^{(1)'}(k_o\rho)\right] \end{aligned}\right\} \tag{6}$$

where A is the amplitude of the electric field, the primes denote derivatives of the Hankel functions with respect to $k_o\rho$, and $n = \frac{\pi}{2\phi_1}$. Because computer programs are readily available for determining integer-order Hankel functions, the flare angle $2\phi_1$ was selected so that n is an integer.

For fixed throat and mouth sizes, two H-plane sectoral horns were constructed for different flare angles. (See fig. 9.) The throat and mouth sizes were 1.016 by 2.286 cm (standard X-band size) and 1.016 by 6.248 cm, respectively. The two flare angles chosen, 18^o and 9^o; and these throat and mouth sizes fix the lengths of the horns at 12.540 and 25.174 cm, respectively. Each horn is terminated in a 30.480-cm-square ground plane. X-band flanges are connected to the throats of the horns.

Experiment

The H-plane sectoral horns were connected to a microwave test setup in the same manner as the pyramidal horn. However, in this case a waveguide-to-waveguide adapter

was not needed since the throat size was the standard X-band waveguide size (1.016 by 2.286 cm).

The reflection coefficients for these horns were measured over a frequency range from 9.0 to 9.6 GHz in 0.2-GHz increments with the horns radiating into free space and into one of the plexiglass or quartz slabs in the pyramidal-horn experiment. For each frequency, the magnitude and phase of the reflection coefficient were plotted as functions of slab thickness. These results are shown in figure 10 for plexiglass and in figure 11 for quartz for the two flare angles of 18° and 9°.

Calculations

The admittance of an H-plane sectoral horn related to the reflection coefficient is determined from equations (6); that is, the wave admittance is defined as follows (see ref. 1, p. 374):

$$Y(k_0\rho) = \frac{H_\phi}{E_z} \tag{7}$$

Substituting H_ϕ and E_z from equations (6) into equation (7) results in

$$Y(k_0\rho) = -jY_0 \frac{H_n^{(2)'}(k_0\rho) + \alpha H_n^{(1)'}(k_0\rho)}{H_n^{(2)}(k_0\rho) + \alpha H_n^{(1)}(k_0\rho)} \tag{8}$$

The characteristic admittance of the sectoral horn is written as

$$Y_c(k_0\rho) = jY_0 \frac{H_n^{(2)'}(k_0\rho)}{H_n^{(2)}(k_0\rho)} \tag{9}$$

Dividing equation (8) by equation (9) gives the normalized wave admittance:

$$\frac{Y(k_0\rho)}{Y_c(k_0\rho)} = -\frac{H_n^{(2)}(k_0\rho)}{H_n^{(2)'}(k_0\rho)} \frac{H_n^{(2)'}(k_0\rho) + \alpha H_n^{(1)'}(k_0\rho)}{H_n^{(2)}(k_0\rho) + \alpha H_n^{(1)}(k_0\rho)} \tag{10}$$

The reflection coefficient in the sectoral horn is defined as

$$\Gamma_s = \alpha \frac{H_n^{(1)}(k_0\rho)}{H_n^{(2)}(k_0\rho)} \tag{11}$$

Solving equation (11) for α and substituting into equation (10) results in the equation

$$\frac{Y(k_o\rho)}{Y_c(k_o\rho)} = -\frac{1 + \Gamma_s \dfrac{H_n^{(2)}(k_o\rho)}{H_n^{(1)}(k_o\rho)} \dfrac{H_n^{(1)'}(k_o\rho)}{H_n^{(2)'}(k_o\rho)}}{1 + \Gamma_s} \tag{12}$$

which may be solved for Γ_s:

$$\Gamma_s = \frac{1 + \dfrac{Y(k_o\rho)}{Y_c(k_o\rho)}}{-\dfrac{Y(k_o\rho)}{Y_c(k_o\rho)} - \dfrac{H_n^{(2)}(k_o\rho)}{H_n^{(1)}(k_o\rho)} \dfrac{H_n^{(1)'}(k_o\rho)}{H_n^{(2)'}(k_o\rho)}} \tag{13}$$

For 18^o and 9^o flare angles, the orders of the Hankel functions are 10 and 20, respectively. At the mouth of the horns $\left(\rho = \rho_2\right)$, the ratio $\dfrac{H_n^{(2)}(k_o\rho_2)}{H_n^{(1)}(k_o\rho_2)} \dfrac{H_n^{(1)'}(k_o\rho_2)}{H_n^{(2)'}(k_o\rho_2)}$ is approximately equal to -1 for $n = 10$ with $k_o\rho_2 = \dfrac{2\pi \times 19.975}{\lambda}$ and for $n = 20$ with $k_o\rho_2 = \dfrac{2\pi \times 39.950}{\lambda}$ over a frequency range from 9.0 to 9.6 GHz. For these conditions, equation (13) becomes

$$\Gamma_s(k_o\rho_2) = \frac{1 + \dfrac{Y(k_o\rho_2)}{Y_c(k_o\rho_2)}}{1 - \dfrac{Y(k_o\rho_2)}{Y_c(k_o\rho_2)}} \tag{14}$$

If the admittance were known at the mouth, the reflection coefficient could be determined at this point from equation (14). The admittance at the mouth is assumed to be approximated by the admittance obtained from equations (1) and (2). Substituting the admittance $Y_{01}y_{11}$ obtained from equation (2a) for the admittance $Y(k_o\rho_2)$ in equation (14) results in the following expression for the reflection coefficient:

$$\Gamma_s = \frac{1 + j\sqrt{1 - \left(\dfrac{\pi}{k_o b}\right)^2} \dfrac{H_n^{(2)}(k_o\rho_2)}{H_n^{(2)'}(k_o\rho_2)} y_{11}}{1 - j\sqrt{1 - \left(\dfrac{\pi}{k_o b}\right)^2} \dfrac{H_n^{(2)}(k_o\rho_2)}{H_n^{(2)'}(k_o\rho_2)} y_{11}} \tag{15}$$

where the characteristic admittance given by equation (9) has been substituted. For the two H-plane horns of the present study, the term $\sqrt{1 - \left(\frac{\pi}{k_o b}\right)^2} \frac{H_n^{(2)}(k_o \rho_2)}{H_n^{(2)'}(k_o \rho_2)}$ is approximately equal to $e^{j\frac{\pi}{2}}$. Therefore, equation (15) with $y_{11} = y_{ap}$ becomes

$$\Gamma_s = \frac{1 - y_{ap}}{1 + y_{ap}} \tag{16}$$

By supplying the parameters a, b, d, ϵ_1, and frequency and by selecting the aperture size to be the same as the mouth size of the H-plane horn (a = 1.016 cm and b = 6.248 cm), the admittance $y_{ap} = y_{11}$ was determined by using equation (2a) for a frequency range from 9.0 to 9.6 GHz in 0.2-GHz increments. These computations were made for free-space conditions (d = 0 cm) and for plexiglass slabs $(\epsilon_1 = 2.55 - j0.01)$ and quartz slabs of thicknesses d varying from 0.1 to 2.0 cm in 0.1-cm increments. Again, small losses were assumed to alleviate the surface-wave problems that occur in the integration when the dielectric constant is lossless.

As for the pyramidal horn, the contribution of the higher order TE_{03} mode is negligible for the chosen aperture size as shown by the calculations for the H-plane horn presented in table III for several slab thicknesses of plexiglass. Therefore, the admittance obtained by assuming only the TE_{01} mode in the aperture is sufficient, and hence, the aperture admittance y_{ap} is equal to y_{11} given by equation (2a).

The reflection coefficient for each H-plane horn is determined from equations (16) and (2a). Measured and calculated values of the magnitude and phase of the reflection coefficient are plotted as functions of slab thickness. These plots are shown in figures 10 and 11 for plexiglass and quartz, respectively.

Discussion of Results

The assumption that the wave incident on the aperture is a plane wave will cause some error in the calculated results because the wave is actually a cylindrical wave. Most of the reflection for an H-plane horn with a small flare angle occurs at the mouth; therefore, the reflection at the throat is small in comparison with the reflection at the mouth. (See ref. 1.)

As shown in figures 10 and 11, excellent agreement was obtained between the measured and calculated reflection coefficients for free-space conditions. However, when the dielectric slabs were attached to the horns, the magnitude of the reflection coefficient

for the measured data was consistently below the calculated data. As in the pyramidal-horn experiment, the inability to clamp the samples snugly to the ground plane and the nonuniformities in the slab samples will cause some errors in the measurements. In addition, the surface waves trapped in the finite slabs could cause errors in the aperture admittance, as discussed previously. However, the measured reflection coefficients are within about 20 percent of the calculated values.

By using equations (4) and (5), the surface-wave conductance was computed and is shown in table IV along with the total conductance and the percentage of surface-wave conductance contained in the total conductance for the same two slab samples used with the pyramidal horn. The percentage of surface-wave conductance for both plexiglass and quartz is much greater for the H-plane horn than for the pyramidal horn; hence, the edges of the finite slabs could have a greater effect on the aperture admittance for the H-plane horn. The surface-wave conductance is greater for the quartz slab than for the plexiglass slab. The data of table IV as well as those of figures 10 and 11 show that better agreement is obtained for the plexiglass slab than for the quartz slab. Thus, the greater the surface-wave conductance, the greater the disagreement.

The E-plane radiation patterns were measured at 9.0 GHz for an H-plane horn radiating into free space, into the 0.322-cm-thick quartz slab (see fig. 12), and into the 0.345-cm-thick plexiglass slab (see fig. 13). The ripples observed in the patterns for the H-plane horn are greater than those observed for the pyramidal horn; hence, the energy trapped for the H-plane horn is greater. (See ref. 13.) The greater the trapped energy, the more strongly the surface wave is coupled into the slab. The amount of ripple for the quartz slab is greater than that for the plexiglass slab; therefore, the surface wave is greater for the quartz slab than for the plexiglass slab. This result is in agreement with the results determined from the surface-wave-conductance computations.

By fixing the H-plane mouth width as 6.248 cm and varying the E-plane mouth height the surface-wave conductance was computed at 9.0 GHz for the two dielectric slabs. A plot of the normalized surface-wave conductance as a function of E-plane mouth height is shown in figure 14 for the 0.322-cm-thick quartz slab and for 0.345-cm-thick plexiglass slab. Similar graphs for different frequencies and thicknesses can be made. As shown previously for the pyramidal horn, the height can be chosen so that the surface-wave conductance is kept at a minimum. Whatever E-plane height is chosen, however, the feeding-waveguide height must be the same in order for the horn to be an H-plane horn.

Theoretically, as the flare angle approaches zero, the H-plane sectoral horn with fixed mouth size would approach a uniform waveguide with a cross section equal to its mouth size; hence, the aperture admittance would be determined by using equations (1) and (2). Therefore, the measured reflection coefficient for the horn with the smaller flare angle (9^{o}) should be closer to the theoretical results. The data of figures 10 and 11,

which include measured reflection coefficients for 9^{o} and 18^{o} flare angles, generally support this conclusion; that is, the measured reflection coefficients for the 9^{o} flare angle more closely approximate the calculated reflection coefficients, especially in magnitude.

In the appendix, the admittance of a rectangular aperture is shown to approach the admittance of a parallel-plate waveguide radiating into a slab of homogeneous material (ref. 14) as the long dimension of the rectangular aperture becomes infinite. This result is shown numerically (for free-space conditions) in table V.

CONCLUDING REMARKS

Variational expressions of the admittance of a uniform rectangular waveguide-fed aperture covered with homogeneous dielectric material (plexiglass or quartz) have been derived. The electric field inside the waveguide was assumed to be a dominant TE_{01} mode plus the first higher order, odd symmetrical mode (the TE_{03} mode). For the aperture sizes of the pyramidal and H-plane horns, the contribution of the TE_{03} mode to the aperture admittance has been shown to be negligible. Hence, the aperture admittance calculated by using only the TE_{01} mode is adequate.

The admittance of a uniform rectangular waveguide-fed aperture has been assumed to approximate the mouth admittance of the pyramidal and H-plane horns. Based on this assumption, measured and calculated reflection coefficients for free-space conditions show good agreement for all horns. Therefore, it is concluded that internal reflections and construction tolerances do not affect the measurements appreciably.

Good agreement was obtained between the measured and calculated reflection coefficients for the pyramidal horn, particularly for the plexiglass slabs. The greatest disagreement, which occurred in the magnitude of the reflection coefficient for a quartz slab, was attributed to the contribution of the surface-wave conductance to the total conductance of the aperture admittance. This contribution was small for both slab samples, but the contribution for the quartz slab was greater than that for the plexiglass slab. Hence, the edges of the finite slabs are more strongly excited and thus possibly influence the aperture admittance.

The reflection coefficient at the mouth of each H-plane sectoral horn has been shown to be approximately equal to $\frac{1 - y_{ap}}{1 + y_{ap}}$, where y_{ap} is the normalized mouth admittance for uniform rectangular waveguide-fed apertures. The agreement between measured and calculated reflection coefficients for the H-plane horn was not as good as the agreement obtained for the pyramidal horn. However, this discrepancy was in theory attributed to the flare angle and to the effect of the surface waves. The reflection coefficients measured for an H-plane horn with a 9^{o} flare angle more closely approximated the

calculated values than did the measured values for an 18° flare angle, particularly in magnitude.

For both plexiglass and quartz slabs, the contribution of surface-wave conductance to the total conductance of the aperture admittance was much greater for the H-plane horn than for the pyramidal horn. Therefore, the edges of the finite slabs could have a greater effect on the aperture admittance of the H-plane horn. This effect could be sufficient to reduce the reflections at the aperture. The data indicate that this is the case.

The assumption that the wave incident on the aperture was a plane wave caused some errors in the calculated reflection coefficients for both the pyramidal and H-plane horns. In addition to this error and to the errors that could have been caused by the trapped surface waves, the inability to clamp the sample snugly to the ground plane and the nonuniformities in the slab samples also caused errors in the measurements.

The admittance of a uniform rectangular waveguide-fed aperture has been shown to approach the admittance of a parallel-plate waveguide radiating into a slab of homogeneous material as the long dimension of the aperture becomes infinite. This result has been shown both analytically and numerically (for free-space conditions) for the dominant mode. Agreement between the two methods of obtaining the admittance of a parallel-plate waveguide supports the validity of the expression for the admittance of a rectangular aperture.

Langley Research Center,
National Aeronautics and Space Administration,
Hampton, Va., June 25, 1970.

APPENDIX

LIMITING OPERATION OF RECTANGULAR-APERTURE ADMITTANCE

The admittance of a rectangular aperture for the dominant TE_{01} mode is given by equation (2a) of the text as

$$Y_{11} = y_{11}Y_{01} = -j\frac{2Y_0k_0^2}{ab(2\pi)^2}\int_{-\infty}^{\infty}\int_{-\infty}^{\infty}\frac{C_0(k_x)C_0(k_x)C_1(k_y)C_1(k_y)}{k_x^2 + k_y^2}$$
$$\times\left[-\left(\frac{k_y}{k_0}\right)^2\frac{g'(0)}{k_0g(0)} + \left(\frac{k_x}{k_0}\right)^2\frac{\epsilon_1}{\epsilon_0}\frac{k_0f(0)}{f'(0)}\right]dk_x\,dk_y \qquad \text{(A1)}$$

where

$$C_0(k_x) = \int_{-a/2}^{a/2} e^{jk_xx}dx = \frac{2\sin\frac{k_xa}{2}}{k_x} \qquad \text{(A2a)}$$

$$C_1(k_y) = \int_{-b/2}^{b/2}\cos\frac{\pi y}{b}\,e^{jk_yy}dy \qquad \text{(A2b)}$$

$$\frac{g'(0)}{g(0)} = \frac{k_z^{II}\sin k_z^{II}d - jk_z^{III}\cos k_z^{II}d}{\cos k_z^{II}d + j\frac{k_z^{III}}{k_z^{II}}\sin k_z^{II}d} \qquad \text{(A2c)}$$

$$\frac{f(0)}{f'(0)} = \frac{\cos k_z^{II}d + j\frac{\epsilon_1}{\epsilon_0}\frac{k_z^{III}}{k_z^{II}}\sin k_z^{II}d}{k_z^{II}\sin k_z^{II}d - j\frac{\epsilon_1}{\epsilon_0}\cos k_z^{II}d} \qquad \text{(A2d)}$$

The purpose of this appendix is to determine what happens to the admittance of the rectangular aperture as the long dimension of the aperture becomes infinite. Analytically, this determination depends on the limit of equation (A1) as b approaches infinity; that is,

$$\lim_{b\to\infty} Y_{11} = \lim_{b\to\infty} -j\frac{2Y_o k_o^2}{ab(2\pi)^2}\int_{-\infty}^{\infty}\int_{-\infty}^{\infty}\frac{C_0(k_x)C_0(k_x)C_1(k_y)C_1(k_y)}{k_x^2+k_y^2}$$

$$\times\left[-\left(\frac{k_y}{k_o}\right)^2\frac{g'(0)}{k_o g(0)}+\left(\frac{k_x}{k_o}\right)^2\frac{\epsilon_1}{\epsilon_o}\frac{k_o f(0)}{f'(0)}\right]dk_x\,dk_y \tag{A3}$$

or

$$\lim_{b\to\infty} Y_{ap} = -j\frac{2Y_o k_o^2}{a(2\pi)^2}\int_{-\infty}^{\infty}\int_{-\infty}^{\infty}\frac{C_0(k_x)C_0(k_x)}{k_x^2+k_y^2}\lim_{b\to\infty}\frac{C_1(k_y)C_1(k_y)}{b}$$

$$\times\left[-\left(\frac{k_y}{k_o}\right)^2\frac{g'(0)}{k_o g(0)}+\left(\frac{k_x}{k_o}\right)^2\frac{\epsilon_1}{\epsilon_o}\frac{k_o f(0)}{f'(0)}\right]dk_x\,dk_y \tag{A4}$$

By using equation (A2b), the limiting term of equation (A4) is written as

$$\left.\begin{aligned}\lim_{b\to\infty}\frac{C_1(k_y)C_1(k_y)}{b} &= \lim_{b\to\infty}\frac{1}{b}\int_{-b/2}^{b/2}\cos\frac{\pi y}{b}\,e^{jk_y y}dy\int_{-b/2}^{b/2}\cos\frac{\pi y}{b}\,e^{jk_y y}dy\\ \text{or}\\ \lim_{b\to\infty}\frac{C_1(k_y)C_1(k_y)}{b} &= \lim_{b\to\infty}\frac{1}{b}\int_{-\infty}^{\infty}\cos\frac{\pi y}{b}\,e^{jk_y y}dy\int_{-\infty}^{\infty}\cos\frac{\pi y}{b}\,e^{jk_y y}\,dy\end{aligned}\right\} \tag{A5}$$

where the two integrals are Fourier transforms of $\cos\frac{\pi y}{b}$. The product of Fourier transforms equals the Fourier transform of the convolution of their inverse transforms; therefore, equation (A5) is written as

$$\left.\begin{aligned}\lim_{b\to\infty}\frac{C_1(k_y)C_1(k_y)}{b} &= \lim_{b\to\infty}\frac{1}{b}F\left\{\cos\frac{\pi y}{b} * \cos\frac{\pi y}{b}\right\}\\ \text{or}\\ \lim_{b\to\infty}\frac{C_1(k_y)C_1(k_y)}{b} &= \lim_{b\to\infty}\frac{1}{b}F\left\{\int_{-\infty}^{\infty}\cos\frac{\pi\tau}{b}\cos\frac{\pi}{b}(y-\tau)d\tau\right\}\end{aligned}\right\} \tag{A6}$$

And hence,

$$\lim_{b\to\infty}\frac{C_1(k_y)C_1(k_y)}{b} = \pi\delta(k_y) \tag{A7}$$

where $\delta(k_y)$ is the Dirac delta function.

Substituting equation (A7) into equation (A4) results in the expression for the aperture admittance for a parallel-plate waveguide:

$$Y_{ap,p} = \lim_{b\to\infty} Y_{ap} = -j\frac{2Y_o k_o^2}{a(2\pi)^2}\int_{k_x=-\infty}^{\infty} C_0(k_x)C_0(k_x)\int_{k_y=-\infty}^{\infty}\frac{\pi\delta(k_y)}{k_x^2+k_y^2}$$

$$\times\left[-\left(\frac{k_y}{k_o}\right)^2\frac{g'(0)}{k_o g(0)}+\left(\frac{k_x}{k_o}\right)^2\frac{\epsilon_1}{\epsilon_o}\frac{k_o f(0)}{f'(0)}\right]dk_x\,dk_y \tag{A8}$$

or

$$Y_{ap,p} = -j\frac{2Y_o k_o^2}{a(2\pi)^2}\int_{k_x=-\infty}^{\infty}\pi C_0(k_x)C_0(k_x)\left[\left(\frac{k_x}{k_o}\right)^2\frac{\epsilon_1}{\epsilon_o}\frac{k_o f(0)}{f'(0)}\right]dk_x \tag{A9}$$

From equations (A2)

$$Y_{ap,p} = \frac{4Y_o}{\pi a}\int_0^{\infty}\frac{\sin^2\frac{k_x a}{2}}{k_x^2}\frac{\epsilon_1}{\epsilon_o}k_o\frac{\cos k_z^{II}d + j\frac{\epsilon_1}{\epsilon_o}\frac{k_z^{III}}{k_z^{II}}\sin k_z^{II}d}{jk_z^{II}\sin k_z^{II}d + \frac{\epsilon_1}{\epsilon_o}k_z^{III}\cos k_z^{II}d}dk_x \tag{A10}$$

The result of dividing both numerator and denominator by $\cos k_z^{II}d$ is

$$Y_{ap,p} = \frac{4}{\pi a}\int_0^{\infty}\frac{\sin^2\frac{k_x a}{2}}{k_x^2}\frac{\omega\epsilon_1}{k_z^{II}}\left(\frac{1+j\frac{\epsilon_1}{\epsilon_o}\frac{k_z^{III}}{k_z^{II}}\tan k_z^{II}d}{\frac{\epsilon_1}{\epsilon_o}\frac{k_z^{III}}{k_z^{II}}+j\tan k_z^{II}d}\right)dk_x \tag{A11}$$

Equation (A11) gives the aperture admittance of a parallel-plate waveguide and with notational changes is identical to the equation given by Jones in reference 14.

The admittance of a rectangular aperture is also shown numerically to approach the admittance of a parallel-plate waveguide with zero thickness of material (free-space conditions). The admittance for $a = 1.016$ cm and a frequency of 8.9 GHz was calculated by using equation (A1) for increasing values of b under free-space conditions. These results are presented in table V and are seen to approach the admittance calculated from the parallel-plate solution given by Jones in reference 14.

REFERENCES

1. Risser, J. R.: Waveguide and Horn Feeds. Microwave Antenna Theory and Design, Samuel Silver, ed., Dover Publ., Inc., 1965, pp. 334-387.

2. Wolff, Edward A.: Antenna Analysis. John Wiley & Sons, Inc., c.1966.

3. Compton, R. T., Jr.: The Admittance of Aperture Antennas Radiating Into Lossy Media. Rep. 1691-5 (NASA Grant No. NsG-448), Antenna Lab., Ohio State Univ. Res. Found., Mar. 15, 1964.

4. Villeneuve, A. T.: Admittance of Waveguide Radiating Into Plasma Environment. IEEE Trans. Antennas Propagation, vol. AP-13, no. 1, Jan. 1965, pp. 115-121.

5. Swift, Calvin T.: Input Admittance of a Rectangular Waveguide-Fed Aperture Antenna Radiating Into an Inhomogeneous Lossy Dielectric Slab. NASA TN D-4197, 1967.

6. Galejs, Janis: Admittance of a Waveguide Radiating Into Stratified Plasma. IEEE Trans. Antennas Propagation, vol. AP-13, no. 1, Jan. 1965, pp. 64-70.

7. Galejs, Janis: Slot Antenna Impedance for Plasma Layers. IEEE Trans. Antennas Propagation, vol. AP-12, no. 6, Nov. 1964, pp. 738-745.

8. Galejs, Janis; and Mentzoni, Michael H.: Waveguide Admittance for Radiation Into Plasma Layers – Theory and Experiment. IEEE Trans. Antennas Propagation, vol. AP-15, no. 3, May 1967, pp. 465-470.

9. Cockrell, C. R.: Higher-Order-Mode Effects on the Aperture Admittance of a Rectangular Waveguide Covered With Dielectric and Plasma Slabs. NASA TN D-4774, 1968.

10. Croswell, William F.; Taylor, William C.; Swift, C. T.; and Cockrell, Capers R.: The Input Admittance of a Rectangular Waveguide-Fed Aperture Under an Inhomogeneous Plasma: Theory and Experiment. IEEE Trans. Antennas Propagation, vol. AP-16, no. 4, July 1968, pp. 475-487.

11. Swift, Calvin T.; and Hatcher, Douglas M.: The Input Admittance of a Rectangular Aperture Antenna Loaded With a Dielectric Plug. NASA TN D-4430, 1968.

12. Croswell, William F.; Rudduck, Roger C.; and Hatcher, Douglas M.: The Admittance of a Rectangular Waveguide Radiating Into a Dielectric Slab. IEEE Trans. Antennas Propagation, vol. AP-15, no. 5, Sept. 1967, pp. 627-633.

13. Knop, Charles M.; and Cohn, George I.: Radiation From an Aperture in a Coated Plane. J. Res. Nat. Bur. Stand., D, vol. 68D, no. 4, Apr. 1964, pp. 363-378.

14. Jones, J. Earl: The Influence of Air-Gap Tolerances on the Admittance of a Dielectric-Coated Slot Antenna. IEEE Trans. Antennas Propagation, vol. AP-17, no. 1, Jan. 1969, pp. 63-68.

TABLE I.- NORMALIZED ADMITTANCE CALCULATIONS, INCLUDING HIGHER ORDER MODE, FOR PYRAMIDAL HORN

Frequency, GHz	Plexiglass thickness, cm	y_{11}	$\frac{-(y_{13}^2)}{y_{33} + y_{03}}$	y_{ap}
10.0	0.5	2.6722 + j0.1567	0.0020 - j0.0136	2.6742 + j0.1431
10.0	1.0	1.1748 + j0.0895	.0002 - j0.0041	1.1750 + j0.0854
10.0	1.5	2.4002 - j0.1443	.0318 - j0.0122	2.4320 - j0.1565
10.2	.5	2.6828 + j0.0489	-.0030 - j0.0108	2.6798 + j0.0381
10.2	1.0	1.1624 + j0.1369	-.0010 - j0.0035	1.1614 + j0.1334
10.2	1.5	2.3099 - j0.3059	.0165 - j0.0275	2.3264 - j0.3334
10.4	.5	2.6781 - j0.0621	-.0057 - j0.0102	2.6724 - j0.0723
10.4	1.0	1.1576 + j0.1909	-.0027 - j0.0014	1.1549 + j0.1895
10.6	1.5	2.1739 - j0.4416	-.0038 - j0.0272	2.1701 - j0.4688

TABLE II.- NORMALIZED CONDUCTANCE CALCULATIONS FOR PYRAMIDAL HORN

Frequency, GHz	Total conductance	Surface-wave conductance	Percent*
Plexiglass slab (0.345 cm)			
10.0	1.9601	0.0972	4.9
10.2	2.0240	.1231	6.1
10.4	2.0810	.1508	7.2
10.6	2.1399	.1792	8.4
Quartz slab (0.322 cm)			
10.0	3.0949	0.3184	10.3
10.2	3.2020	.3771	11.8
10.4	3.2970	.4294	13.0
10.6	3.3814	.4709	13.9

*Percentage of surface-wave conductance contained in total conductance.

TABLE III.- NORMALIZED ADMITTANCE CALCULATIONS, INCLUDING HIGHER ORDER MODE, FOR H-PLANE HORN

Frequency, GHz	Plexiglass thickness, cm	y_{11}	$\frac{-(y_{13}^2)}{y_{33} + y_{03}}$	y_{ap}
8.4	0.5	2.1530 + j1.1086	0.00050 - j0.00070	2.1535 + j1.1079
8.4	1.0	1.5356 + j0.2477	.0008 + j0.00009	1.5364 + j0.2478
8.4	1.5	1.5863 + j0.9128	-.00030 + j0.00070	1.5860 + j0.9135
8.6	.5	2.2144 + j1.0467	.00030 - j0.00050	2.2147 + j1.0462
8.6	1.0	1.5147 + j0.2773	-.00002 - j0.00009	1.5147 + j0.2772
8.6	1.5	1.6677 + j0.9173	.00007 + j0.00049	1.6678 + j0.9178
8.8	.5	2.2717 + j0.9794	.00008 - j0.00059	2.2718 + j0.9788
8.8	1.0	1.4931 + j0.2824	-.00004 + j0.00009	1.4931 + j0.2825
8.8	1.5	1.7588 + j0.9029	-.00032 - j0.00073	1.7585 + j0.9022

TABLE IV.- NORMALIZED CONDUCTANCE CALCULATIONS FOR H-PLANE HORN

Frequency, GHz	Total conductance	Surface-wave conductance	Percent*
Plexiglass slab (0.345 cm)			
9.0	1.7333	0.7554	43.6
9.2	1.7884	.7795	43.6
9.4	1.8429	.8024	43.5
9.6	1.8950	.8245	43.5
Quartz slab (0.322 cm)			
9.0	2.6525	1.3358	50.3
9.2	2.7512	1.3879	50.4
9.4	2.8482	1.4365	50.4
9.6	2.9421	1.4807	50.3

*Percentage of surface-wave conductance contained in total conductance.

TABLE V.- NORMALIZED ADMITTANCE CALCULATIONS FOR PARALLEL PLATE, FREE-SPACE CONDITIONS

[Frequency = 8.9 GHz; a = 1.016 cm]

Dimension b, cm	Normalized admittance
2.286	0.7935 + j0.4058
3.286	.7618 + j0.4784
4.286	.7794 + j0.4957
5.286	.8059 + j0.4997
6.248	.8020 + j0.5010
6.348	.8024 + j0.5011
8.000	.8086 + j0.5014
9.000	.8109 + j0.5011
10.000	.8126 + j0.5009
11.000	.8139 + j0.5001
16.000	.8171 + j0.5002
Normalized admittance calculated from parallel-plate solution of reference 14	0.8177 + j0.5035

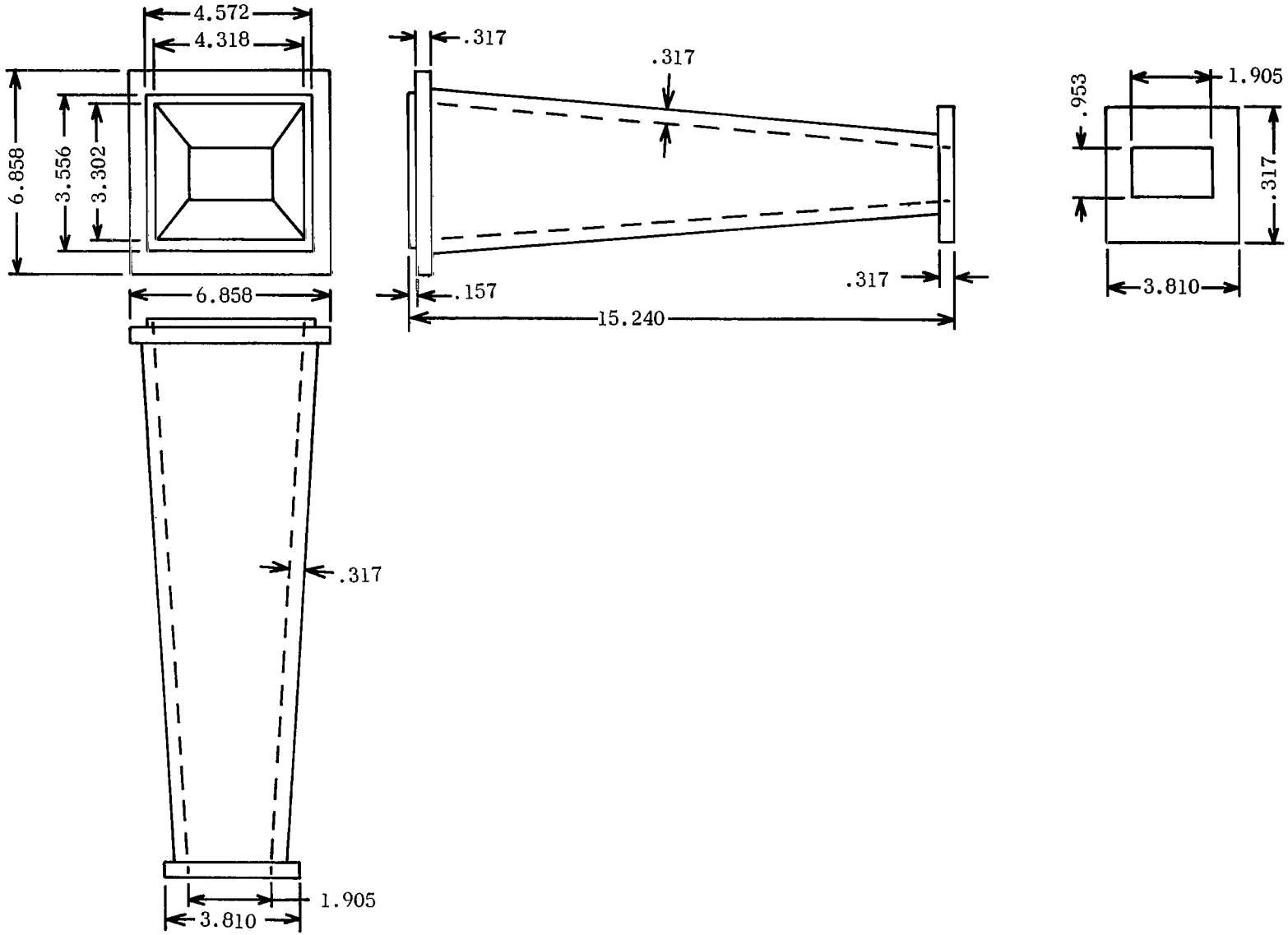

Figure 1.- Details of pyramidal horn. Dimensions are in centimeters.

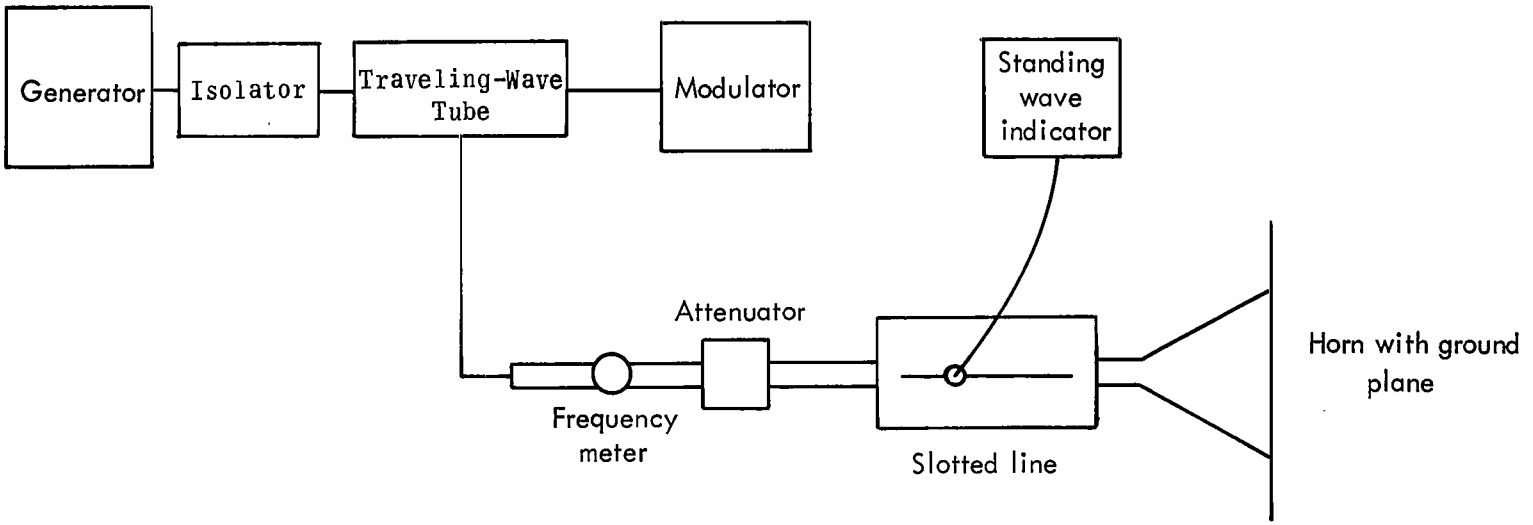

Figure 2.- Schematic drawing of microwave test setup.

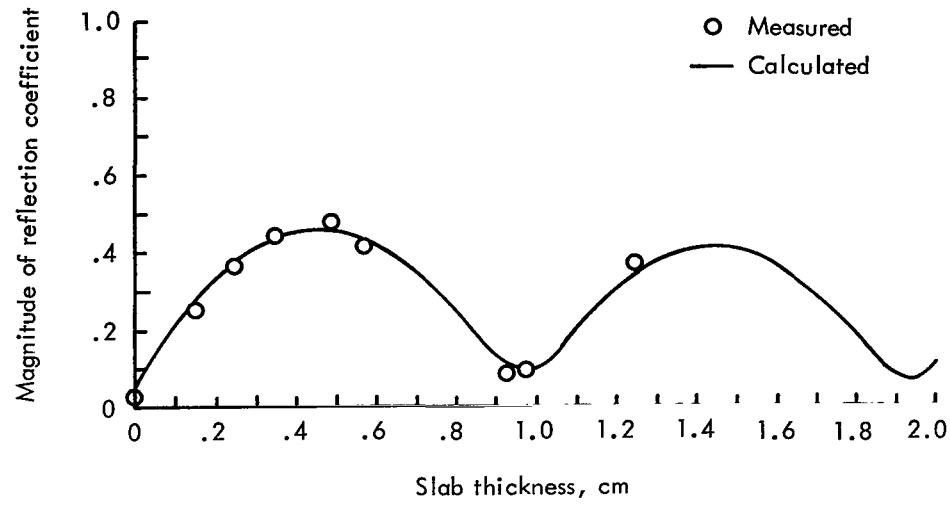

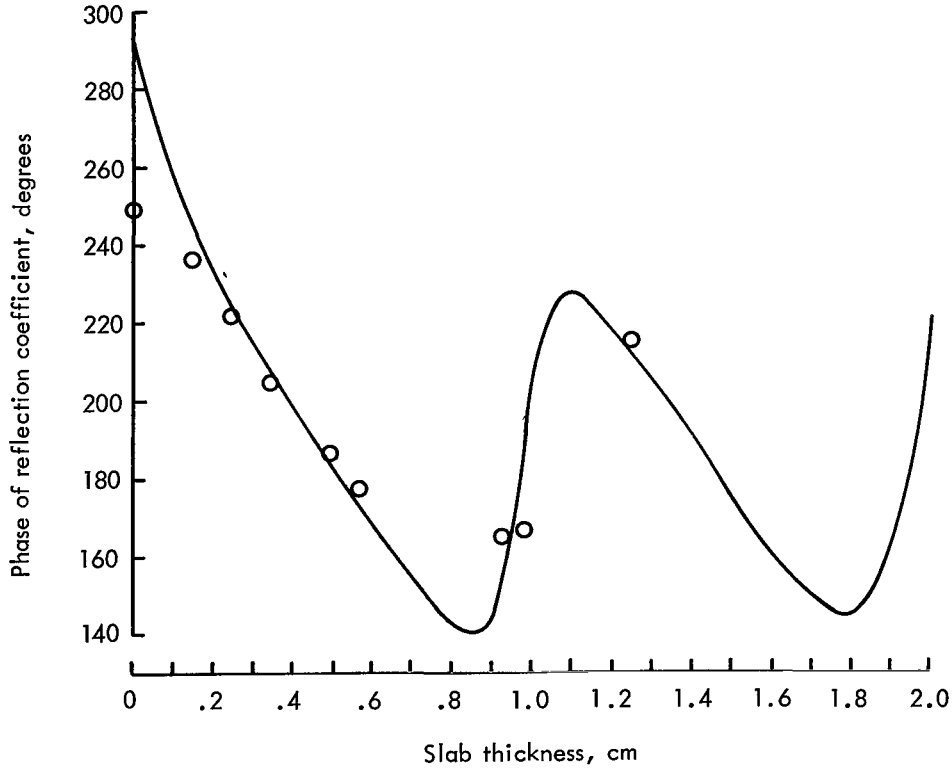

(a) Frequency = 10.0 GHz.

Figure 3.- Reflection coefficient for pyramidal horn as a function of slab thickness for plexiglass.

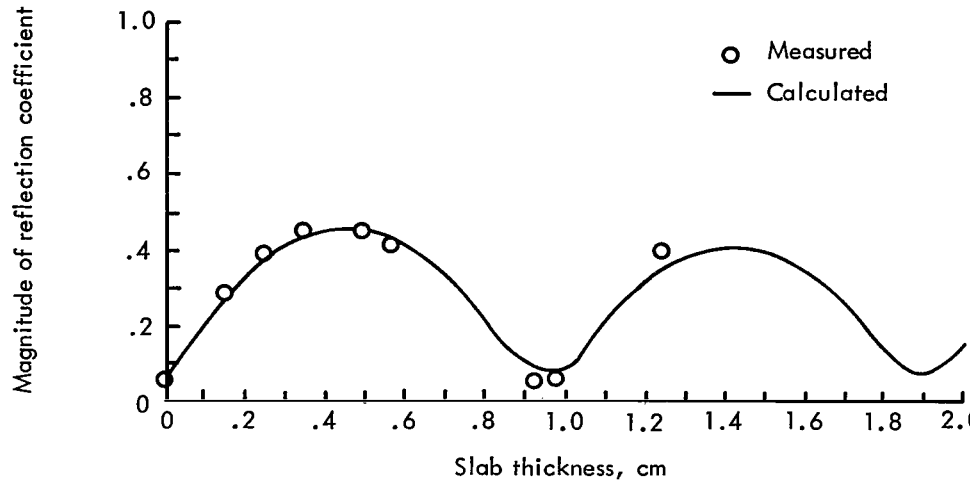

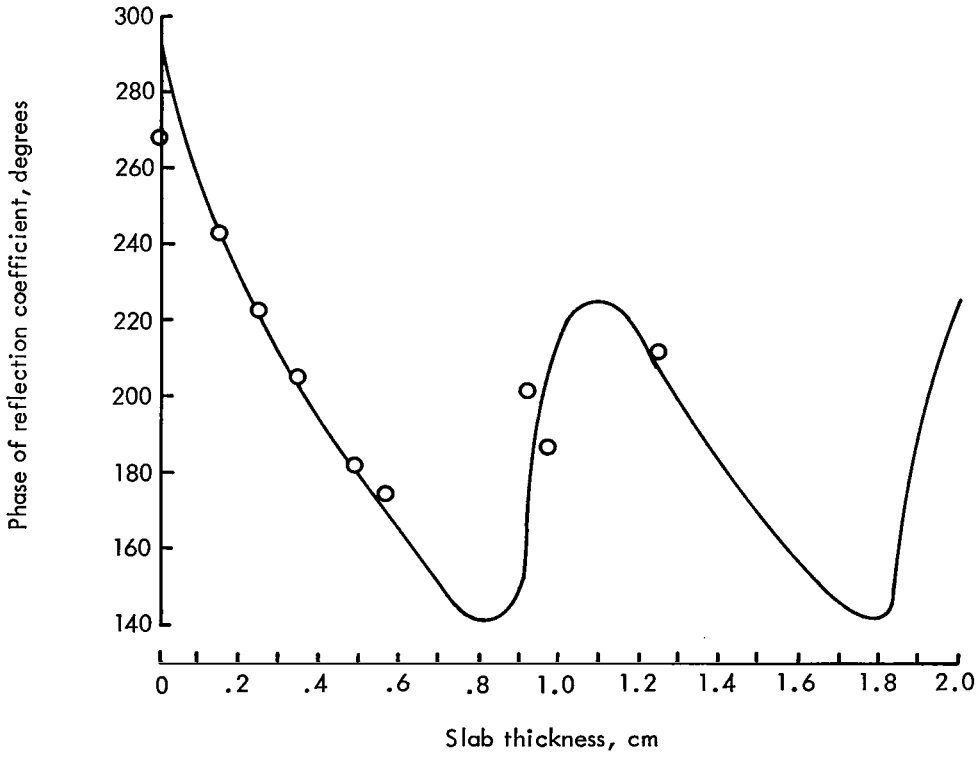

(b) Frequency = 10.2 GHz.

Figure 3.- Continued.

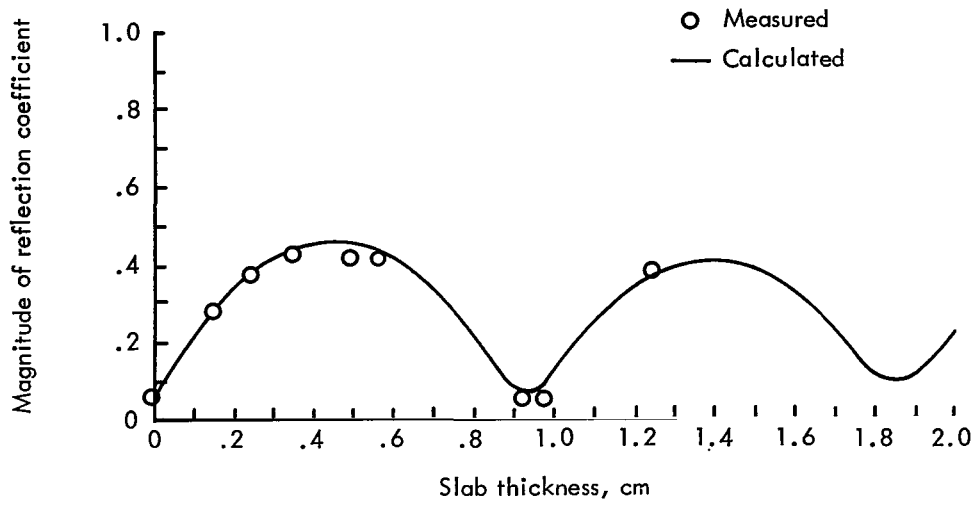

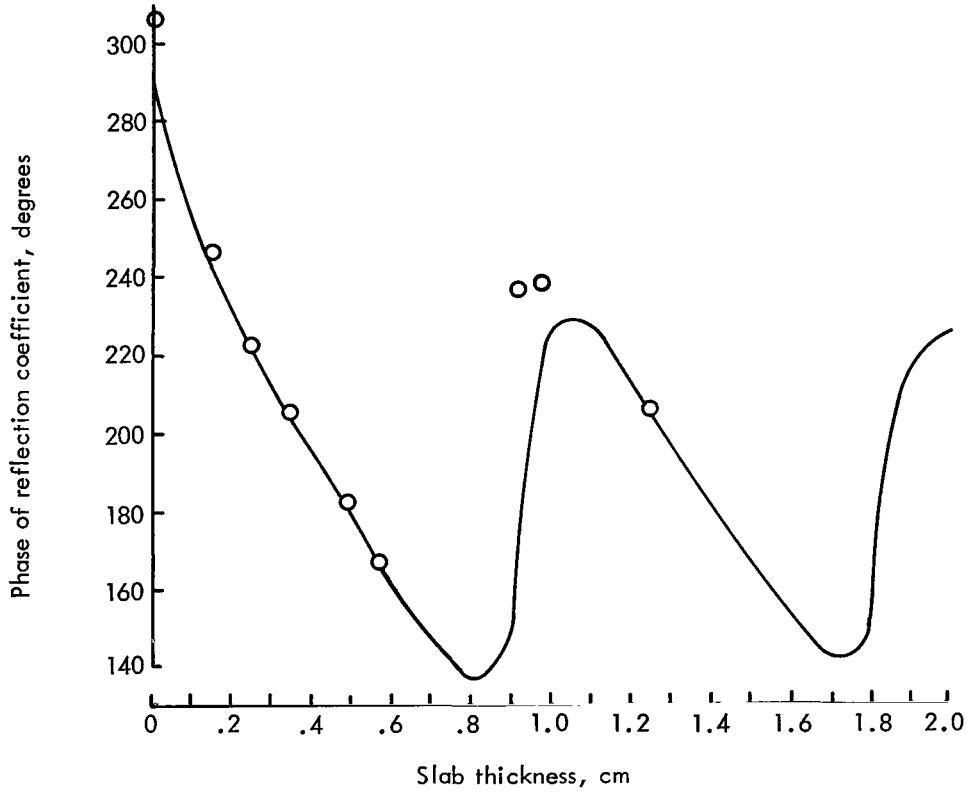

(c) Frequency = 10.4 GHz.

Figure 3.- Continued.

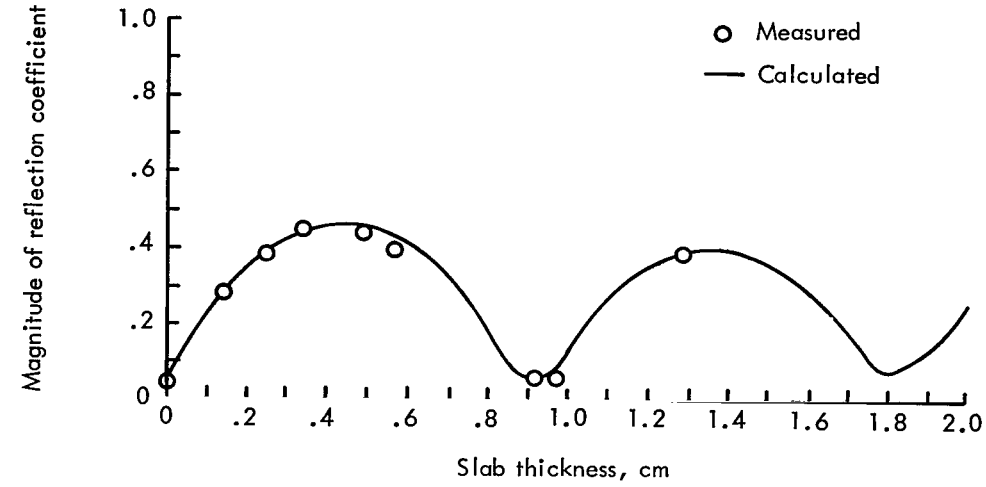

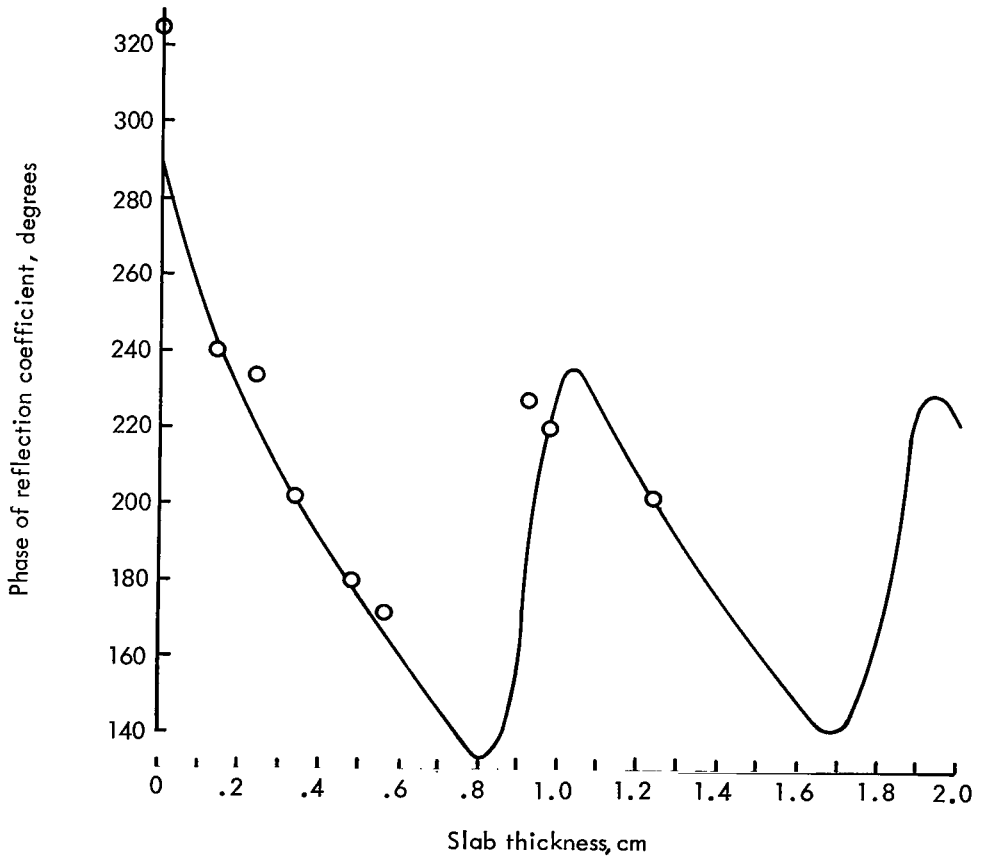

(d) Frequency = 10.6 GHz.

Figure 3.- Concluded.

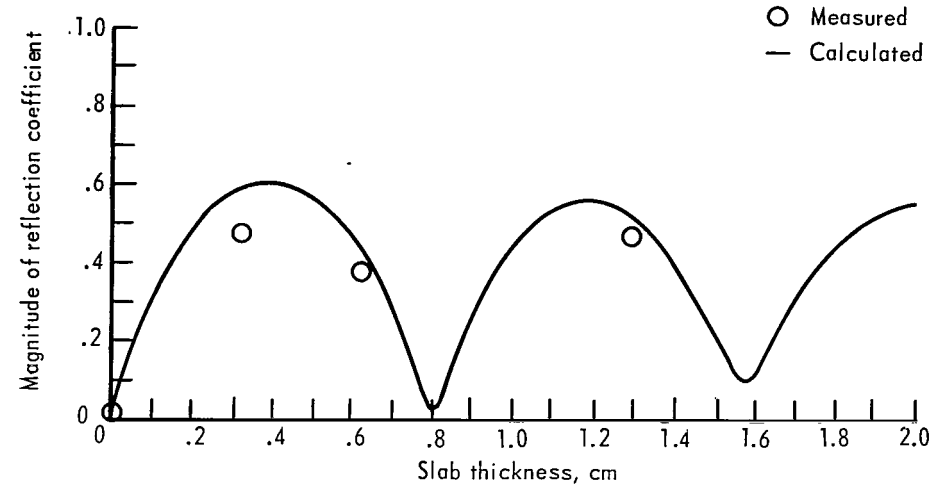

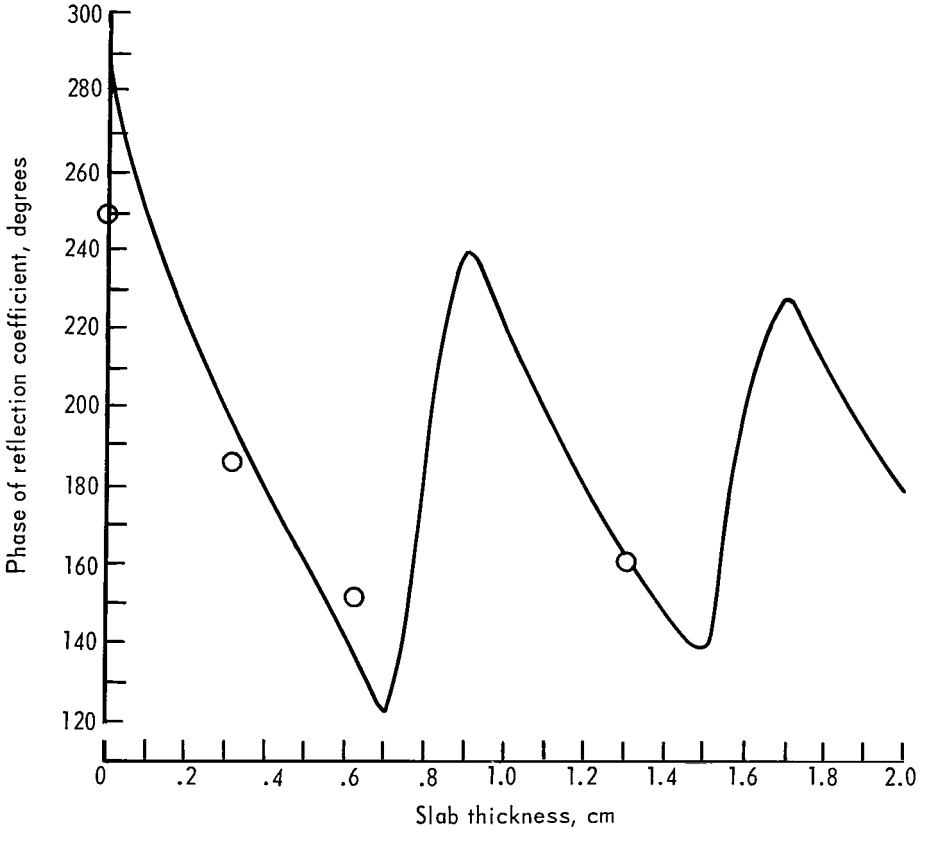

(a) Frequency = 10.0 GHz.

Figure 4.- Reflection coefficient for pyramidal horn as a function of slab thickness for quartz.

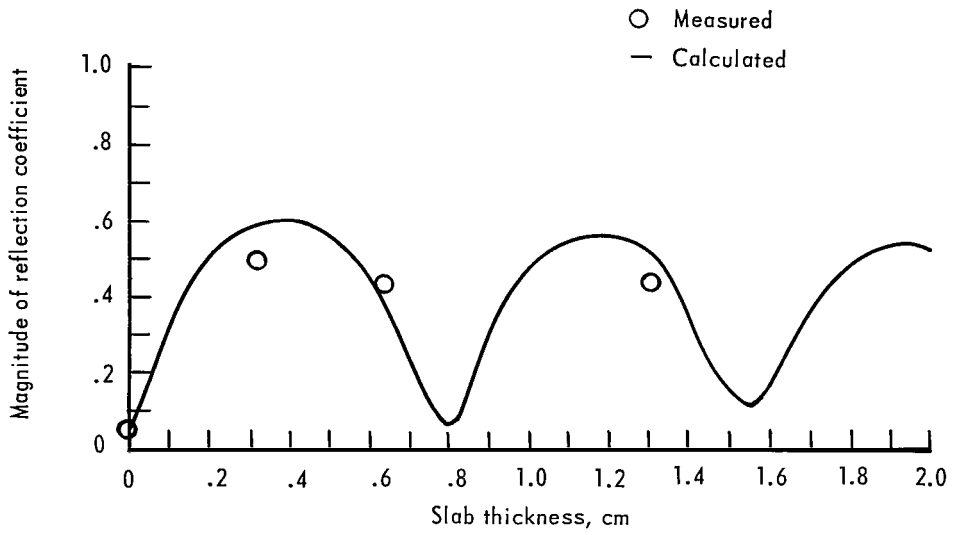

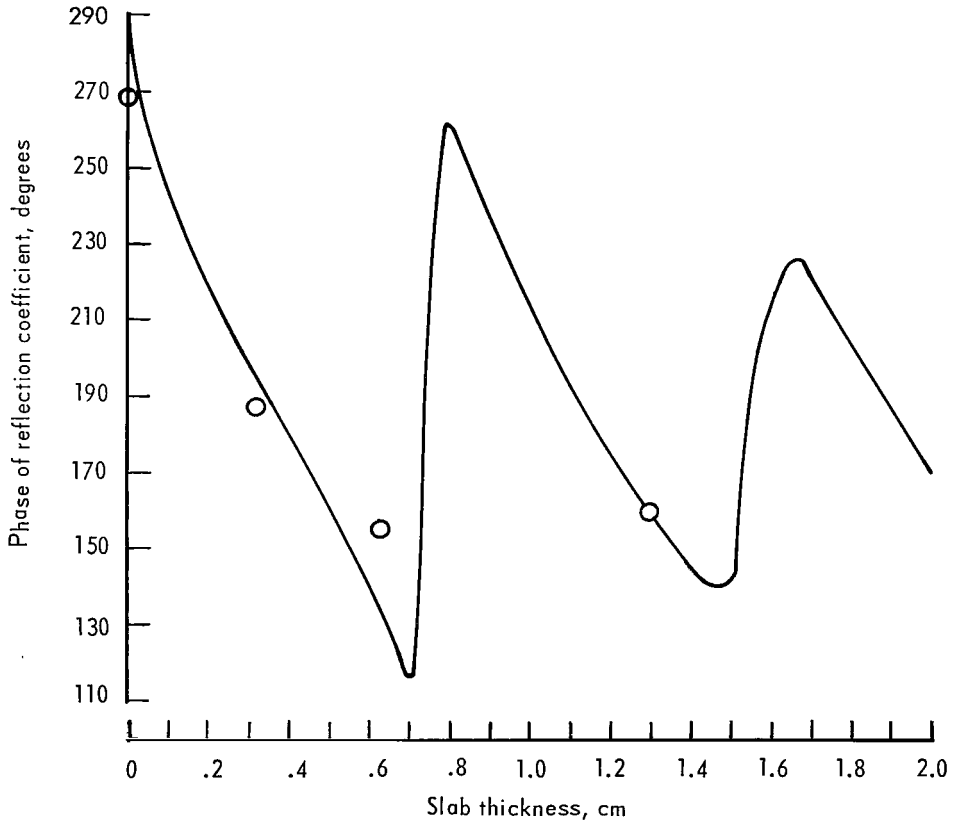

(b) Frequency = 10.2 GHz.

Figure 4.- Continued.

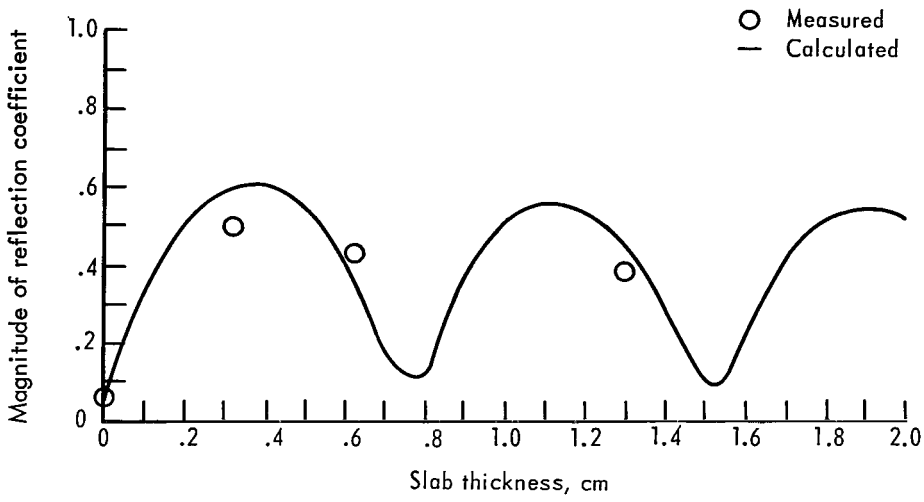

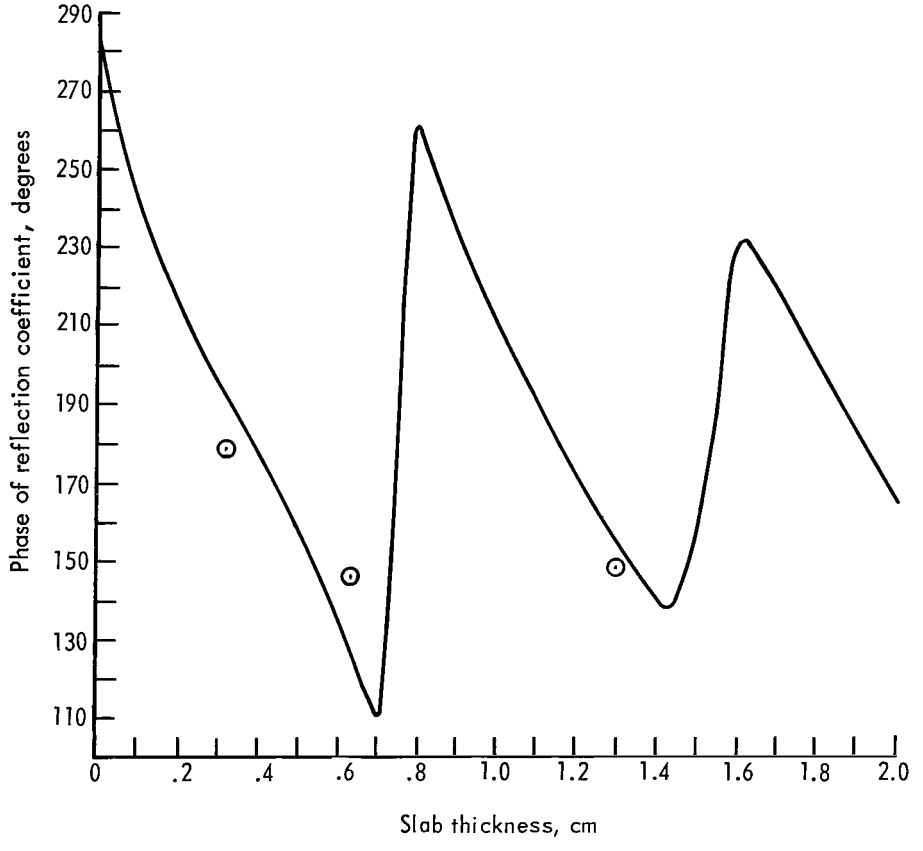

(c) Frequency = 10.4 GHz.

Figure 4.- Continued.

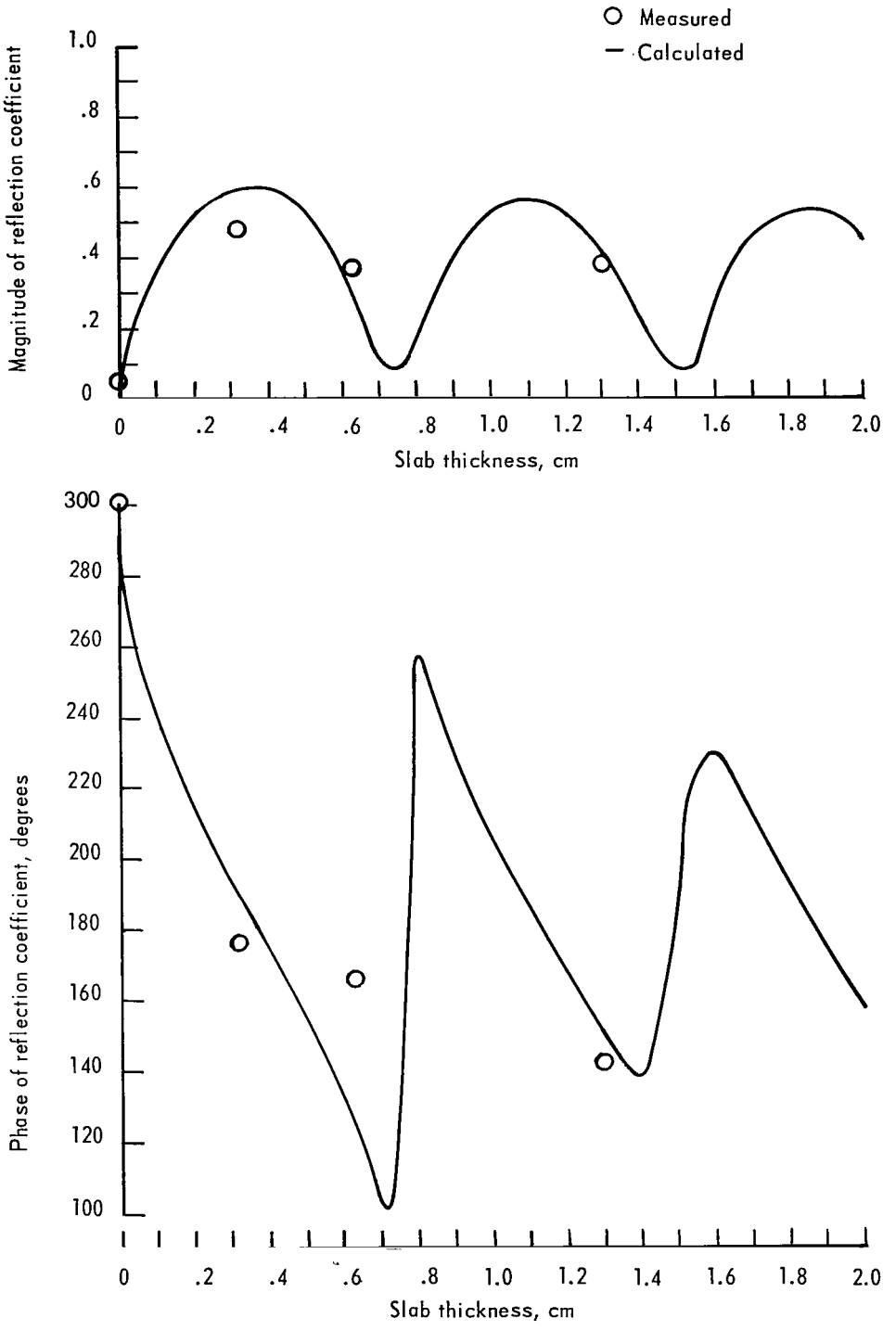

(d) Frequency = 10.6 GHz.

Figure 4.- Concluded.

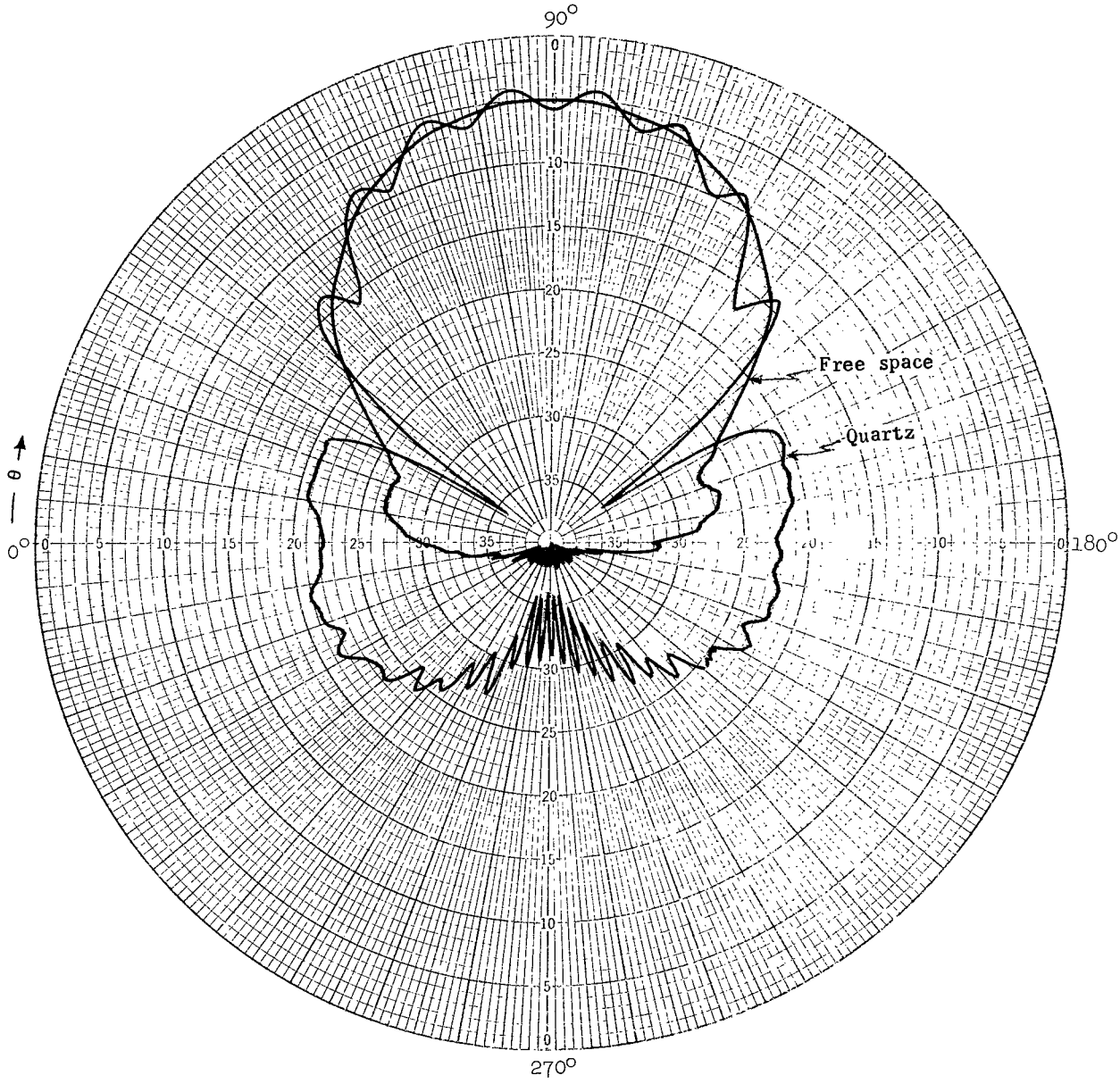

Figure 5.- E-plane radiation pattern at 10.0 GHz for pyramidal horn radiating into free space and into 0.322-cm-thick quartz slab.

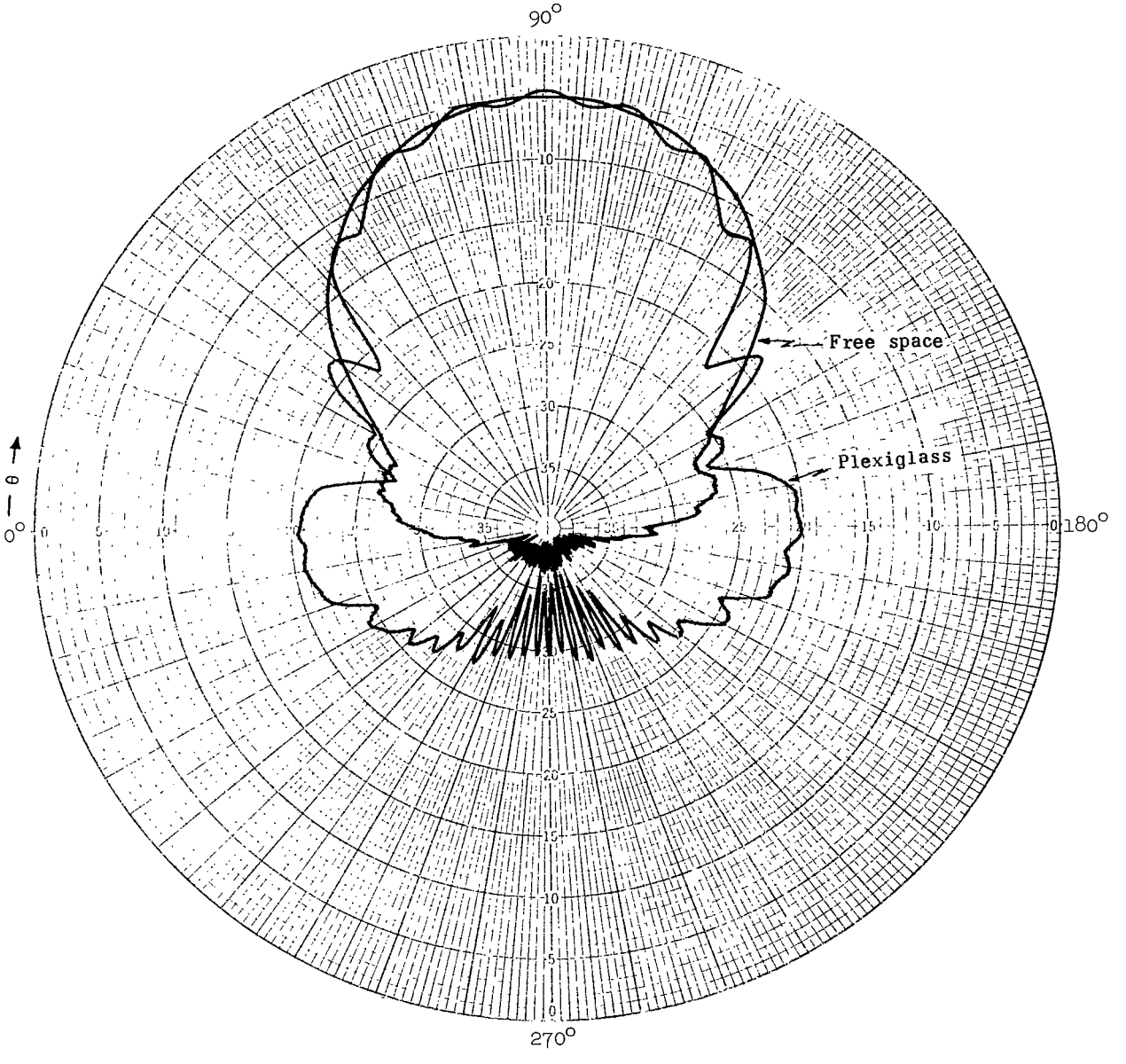

Figure 6.- E-plane radiation pattern at 10.0 GHz for pyramidal horn radiating into free space and into 0.345-cm-thick plexiglass slab.

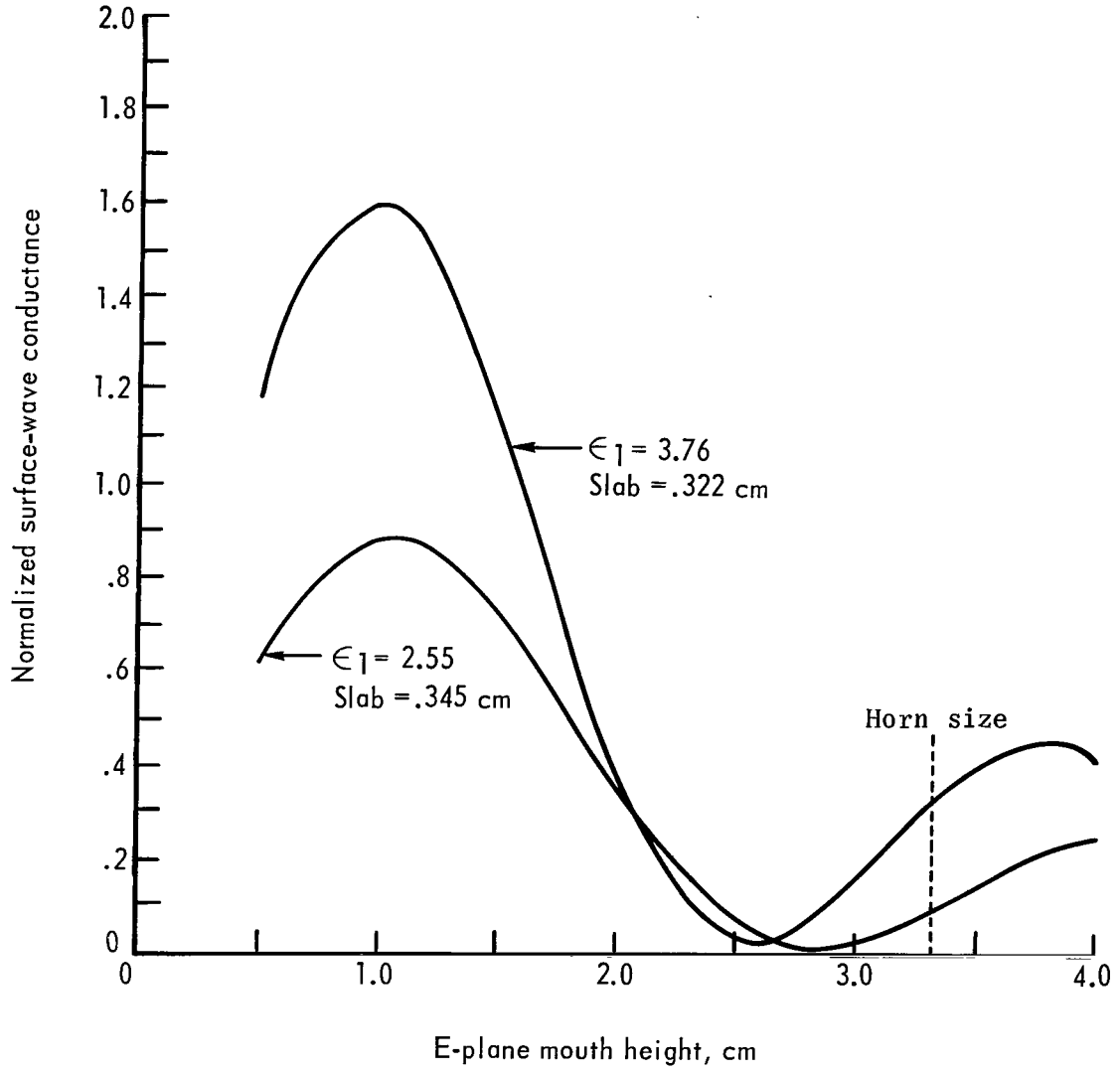

Figure 7.- Normalized surface-wave conductance at 10.0 GHz for pyramidal horn as a function of E-plane mouth height. H-plane mouth width = 4.318 cm.

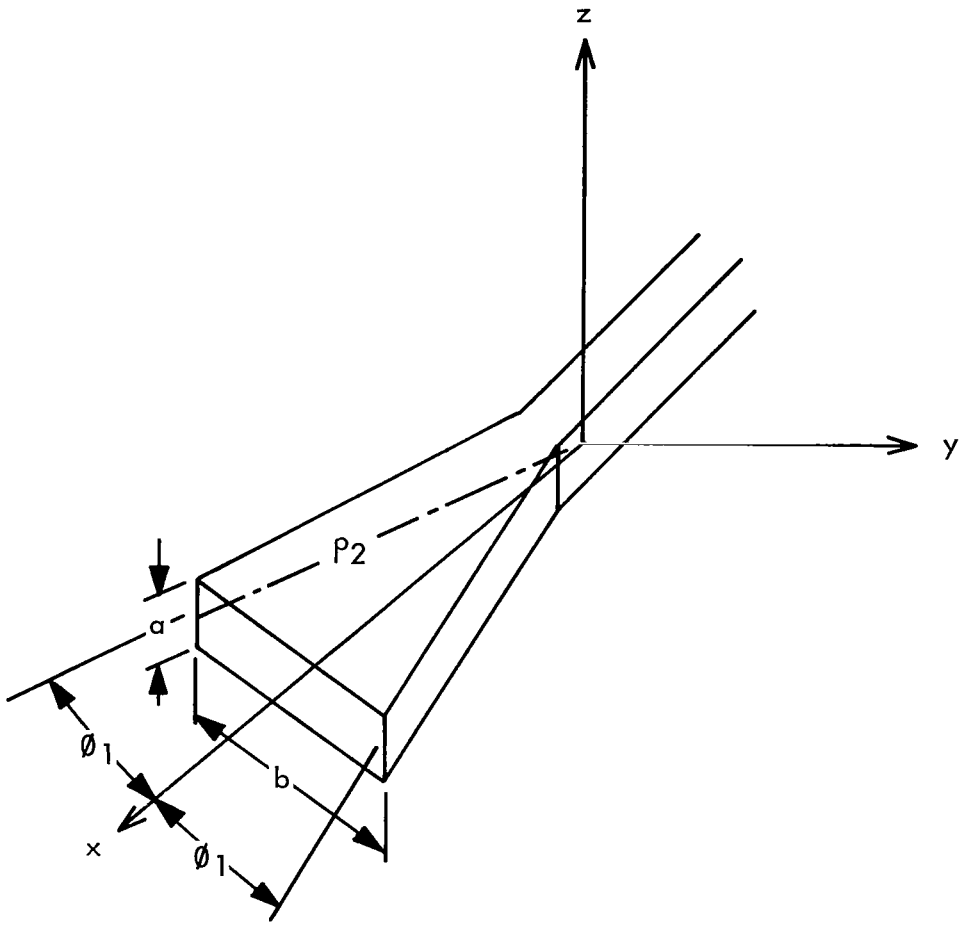

Figure 8.- Sketch of H-plane sectoral horn.

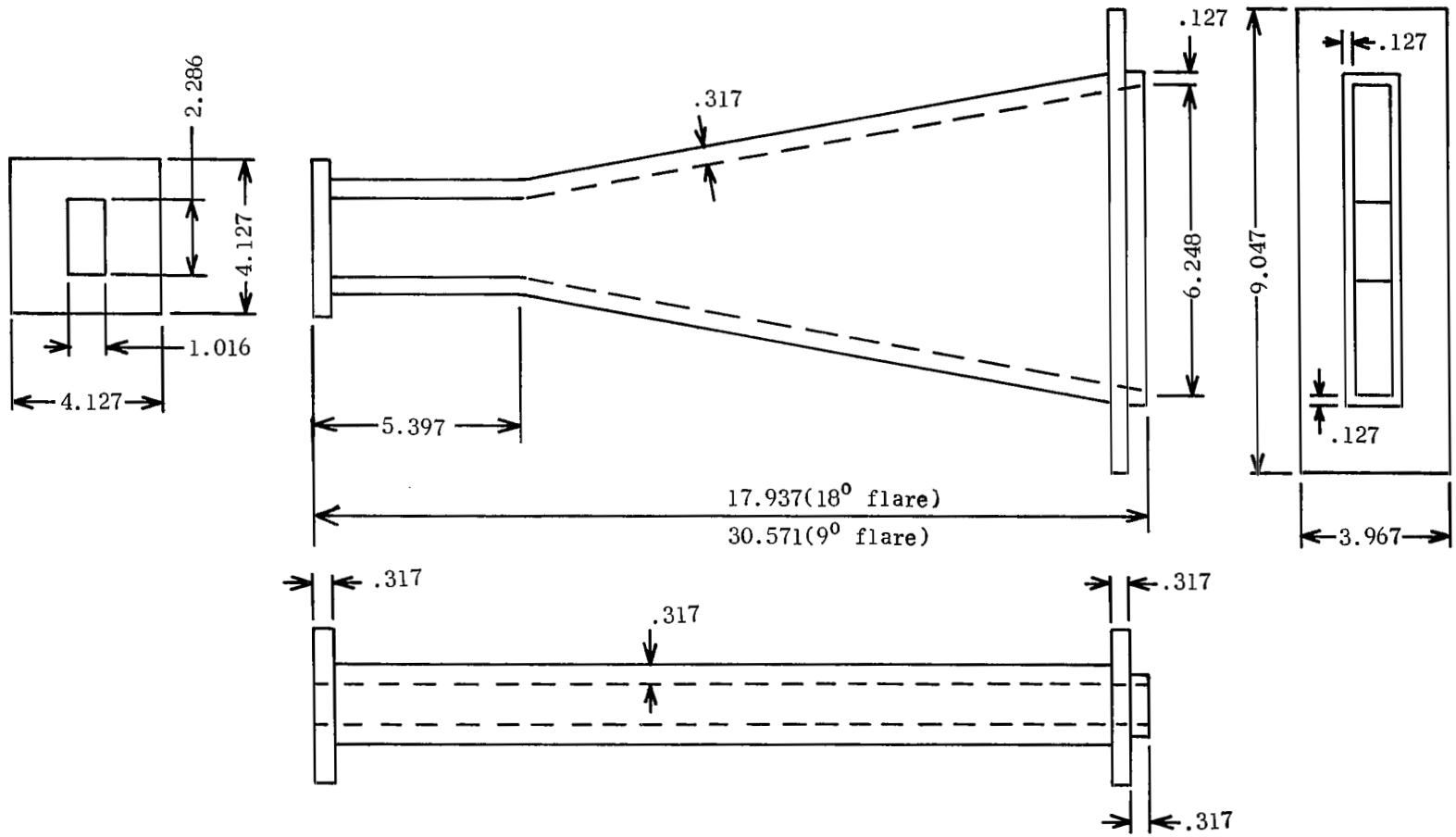

Figure 9.- Details of H-plane sectoral horn. Dimensions are in centimeters.

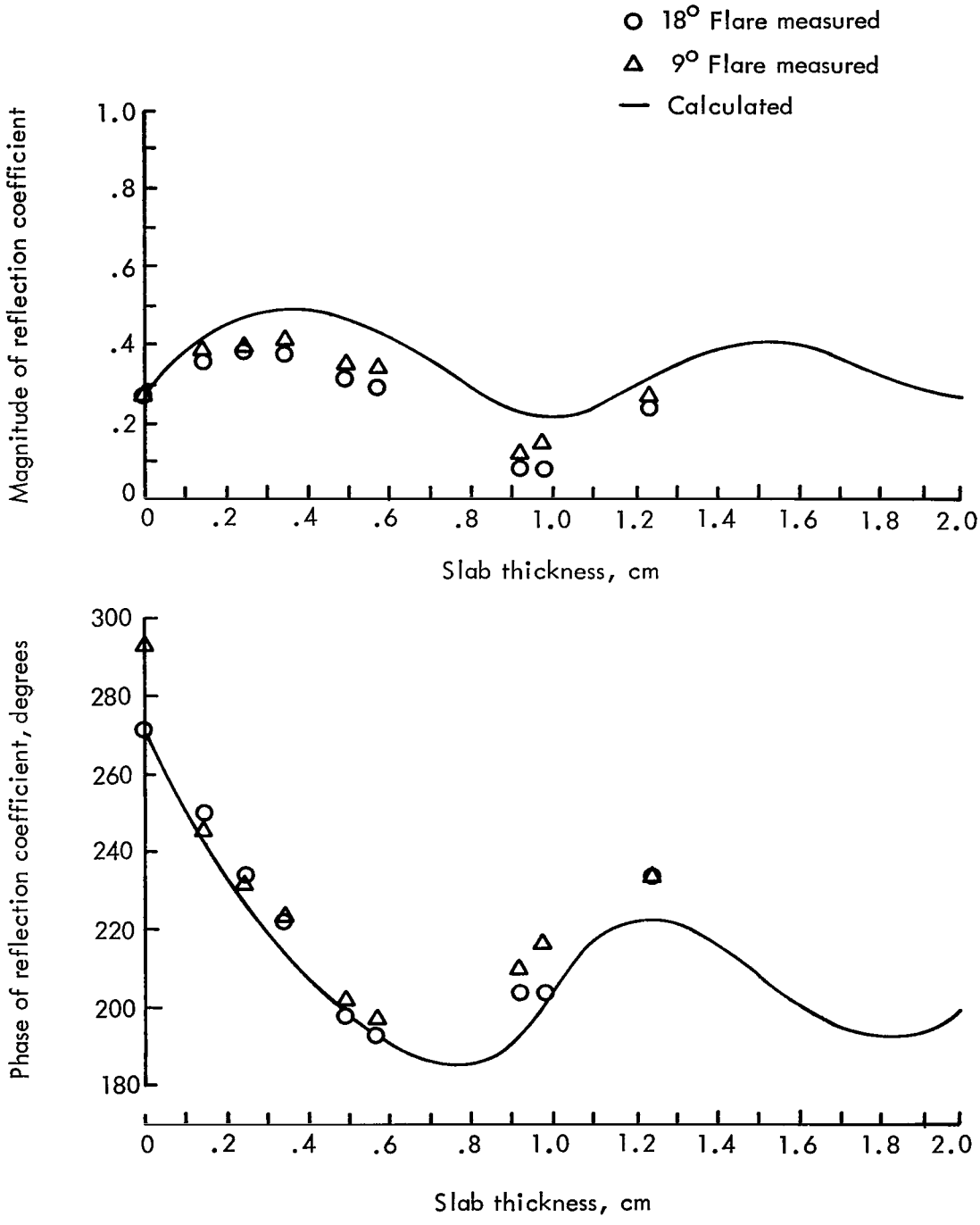

(a) Frequency = 9.0 GHz.

Figure 10.- Reflection coefficient for H-plane sectoral horn as a function of slab thickness for plexiglass.

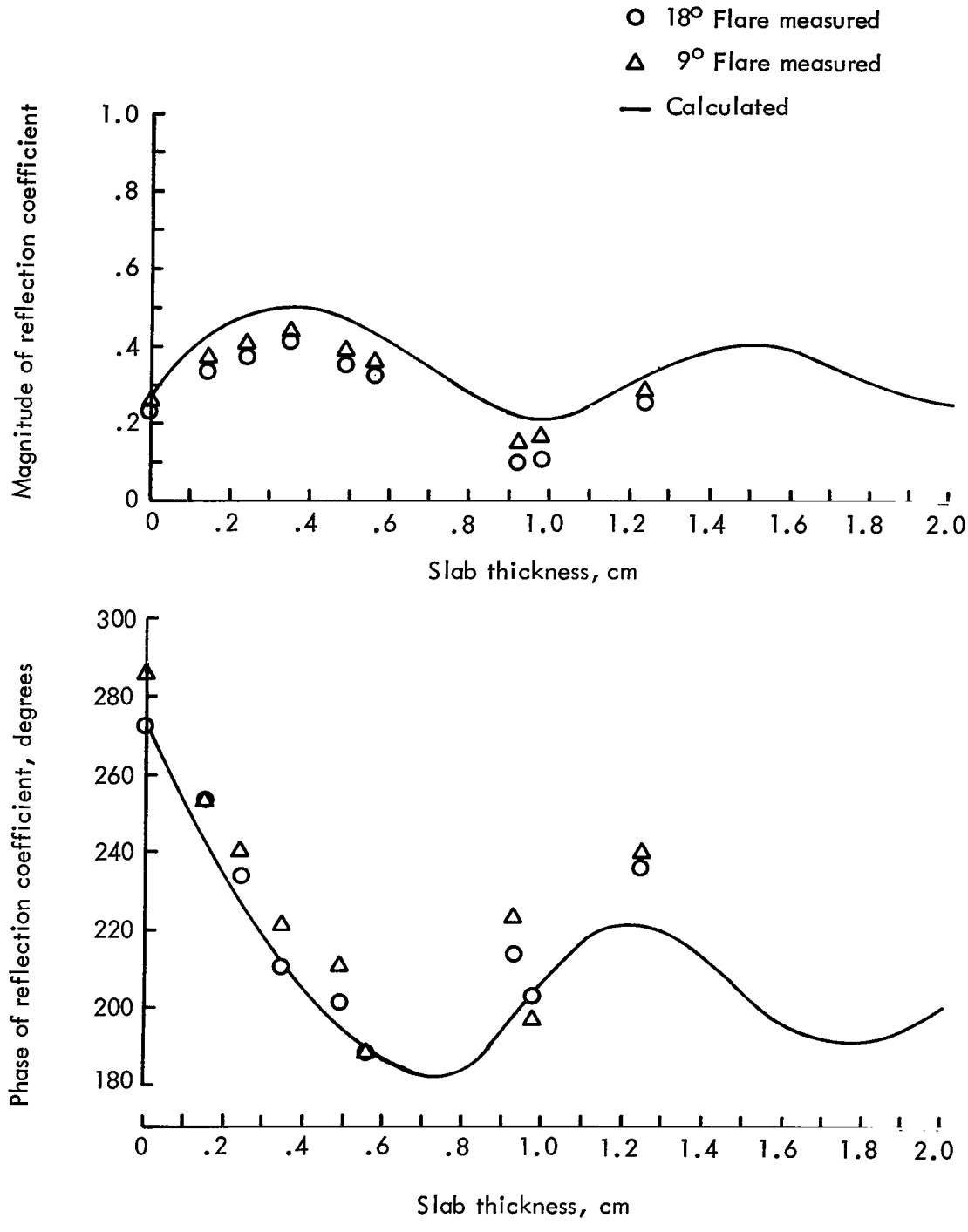

(b) Frequency = 9.2 GHz.

Figure 10.- Continued.

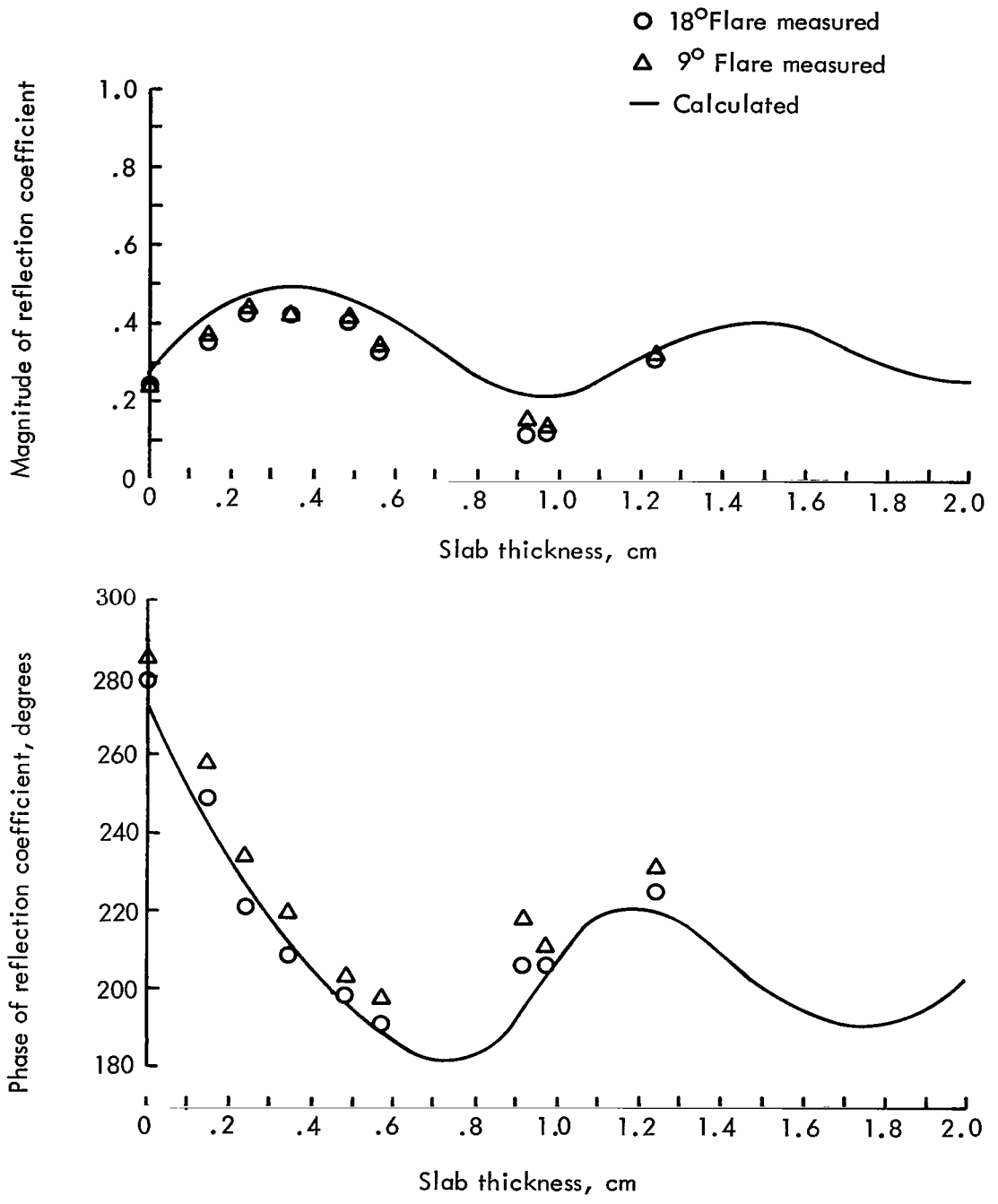

(c) Frequency = 9.4 GHz.

Figure 10.- Continued.

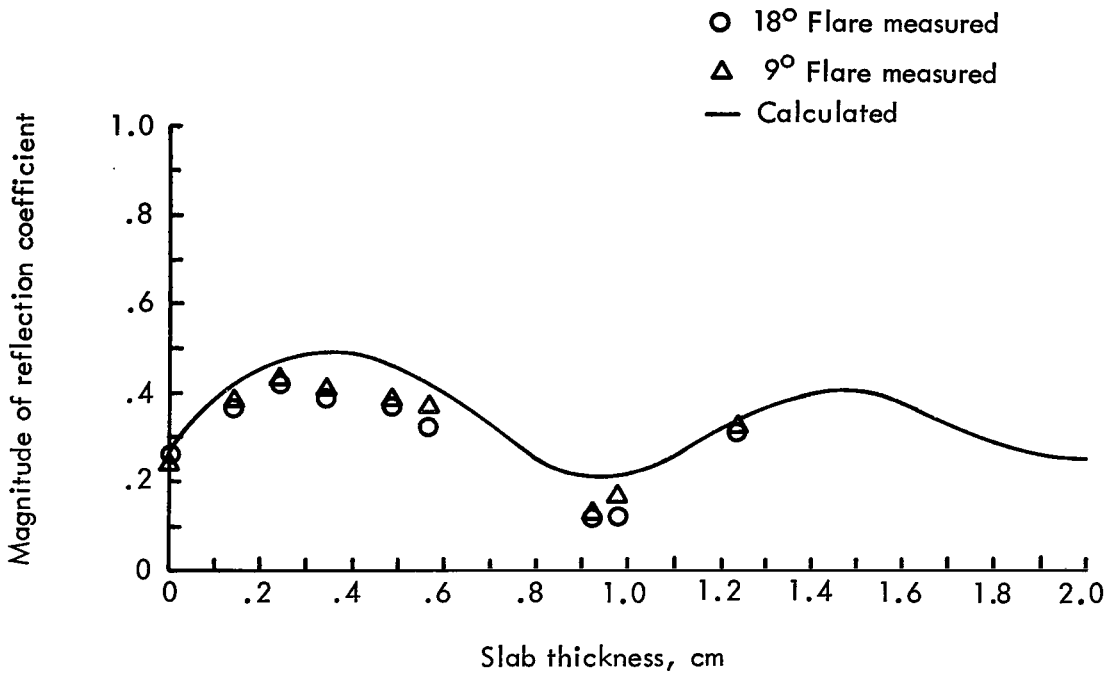

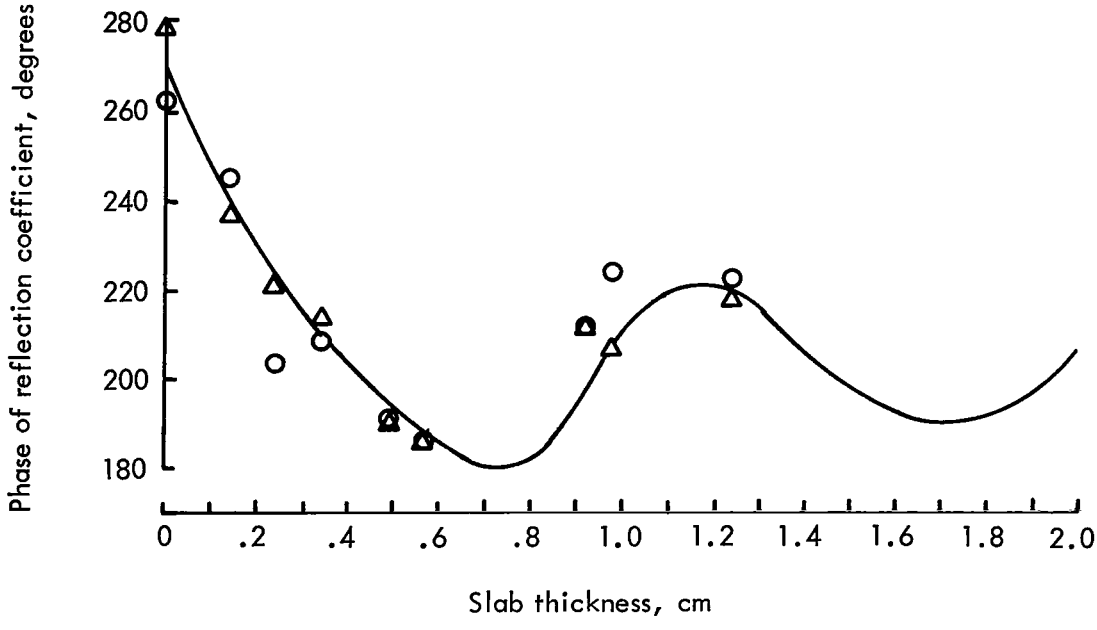

(d) Frequency = 9.6 GHz.

Figure 10.- Concluded.

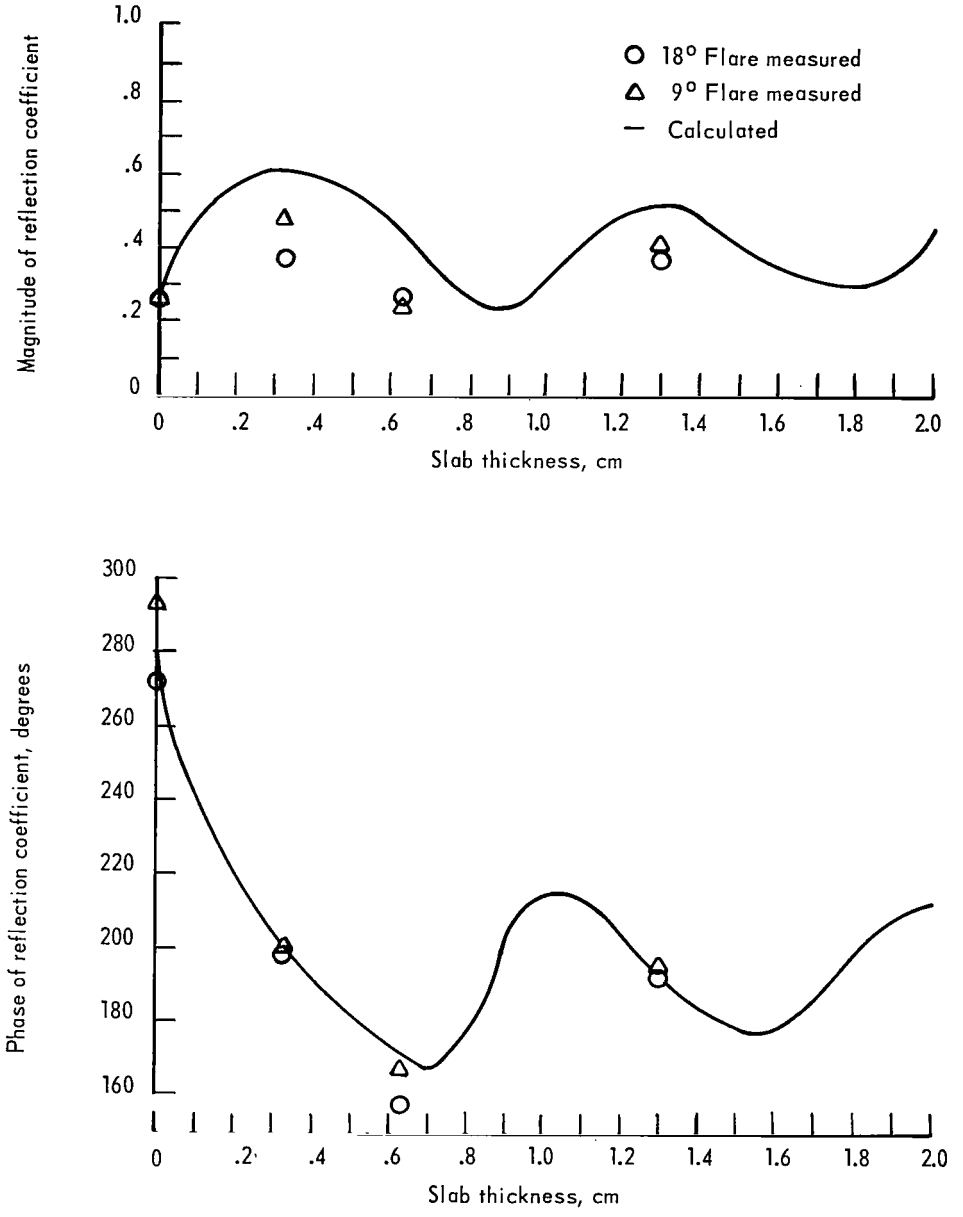

(a) Frequency = 9.0 GHz.

Figure 11.- Reflection coefficient for H-plane sectoral horn as a function of slab thickness for quartz.

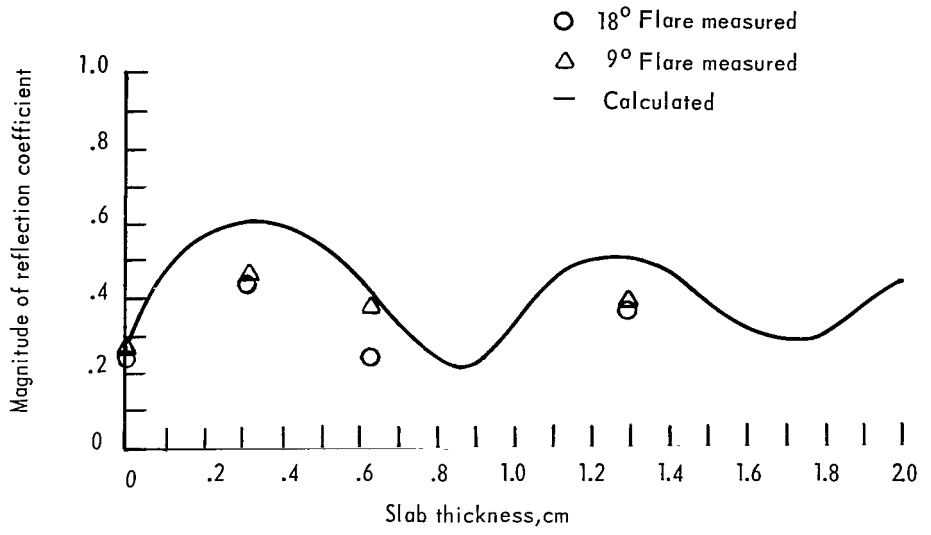

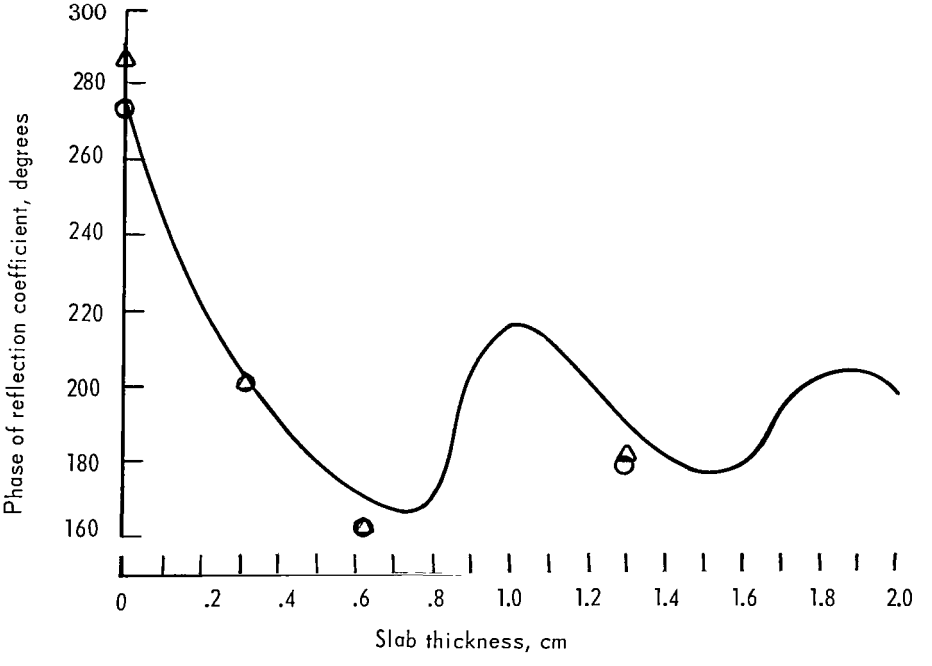

(b) Frequency = 9.2 GHz.

Figure 11.- Continued.

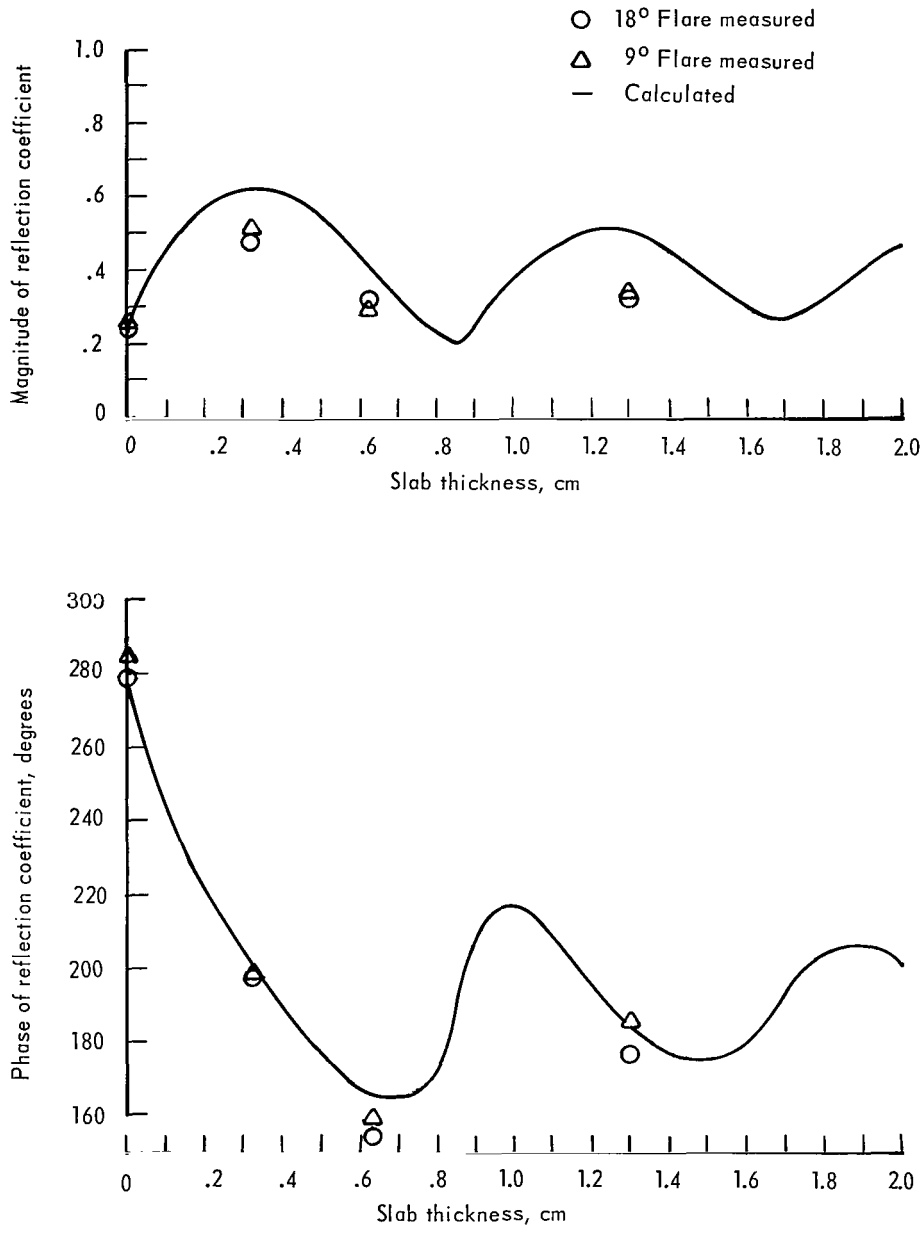

(c) Frequency = 9.4 GHz.

Figure 11.- Continued.

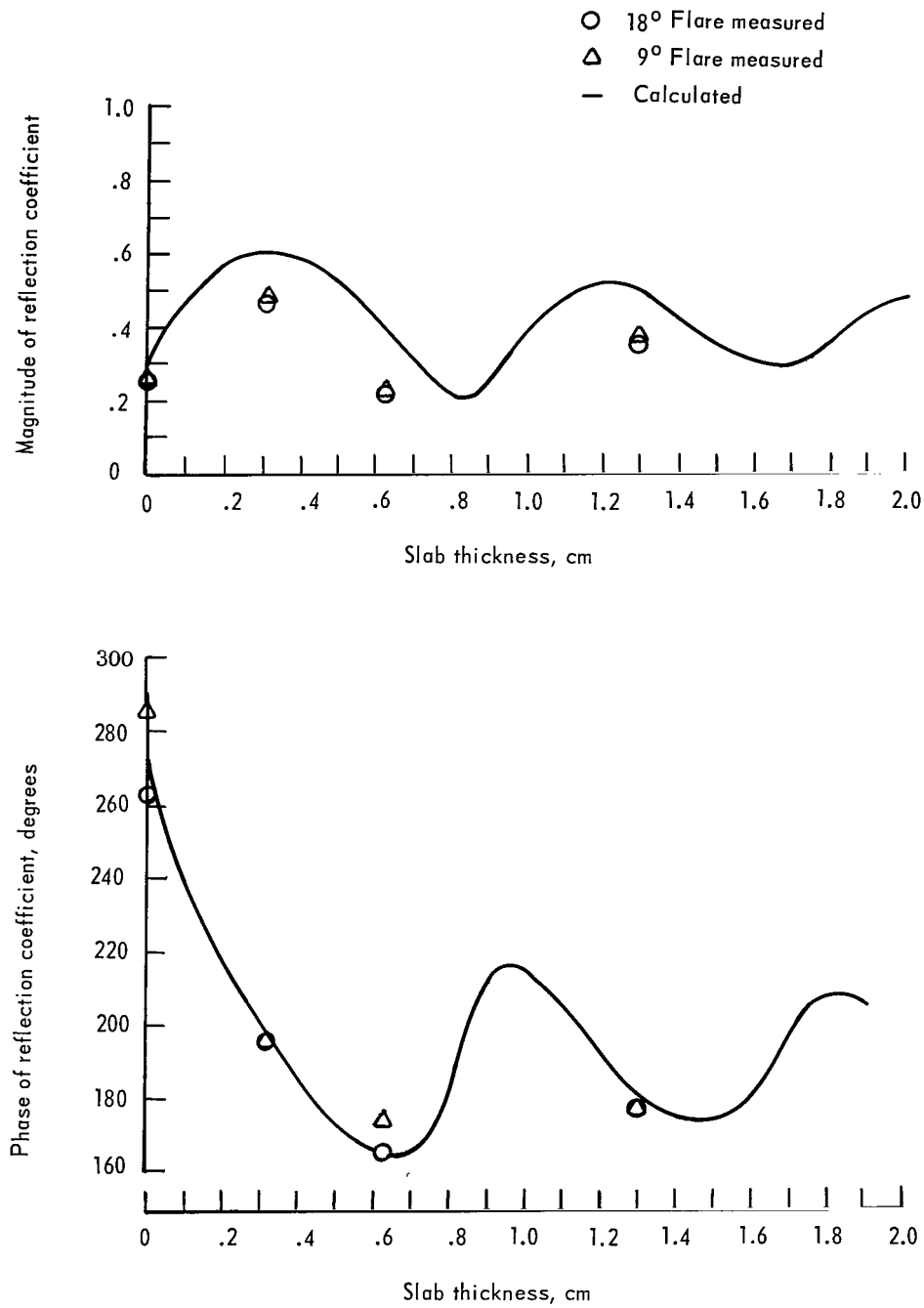

(d) Frequency = 9.6 GHz.

Figure 11.- Concluded.

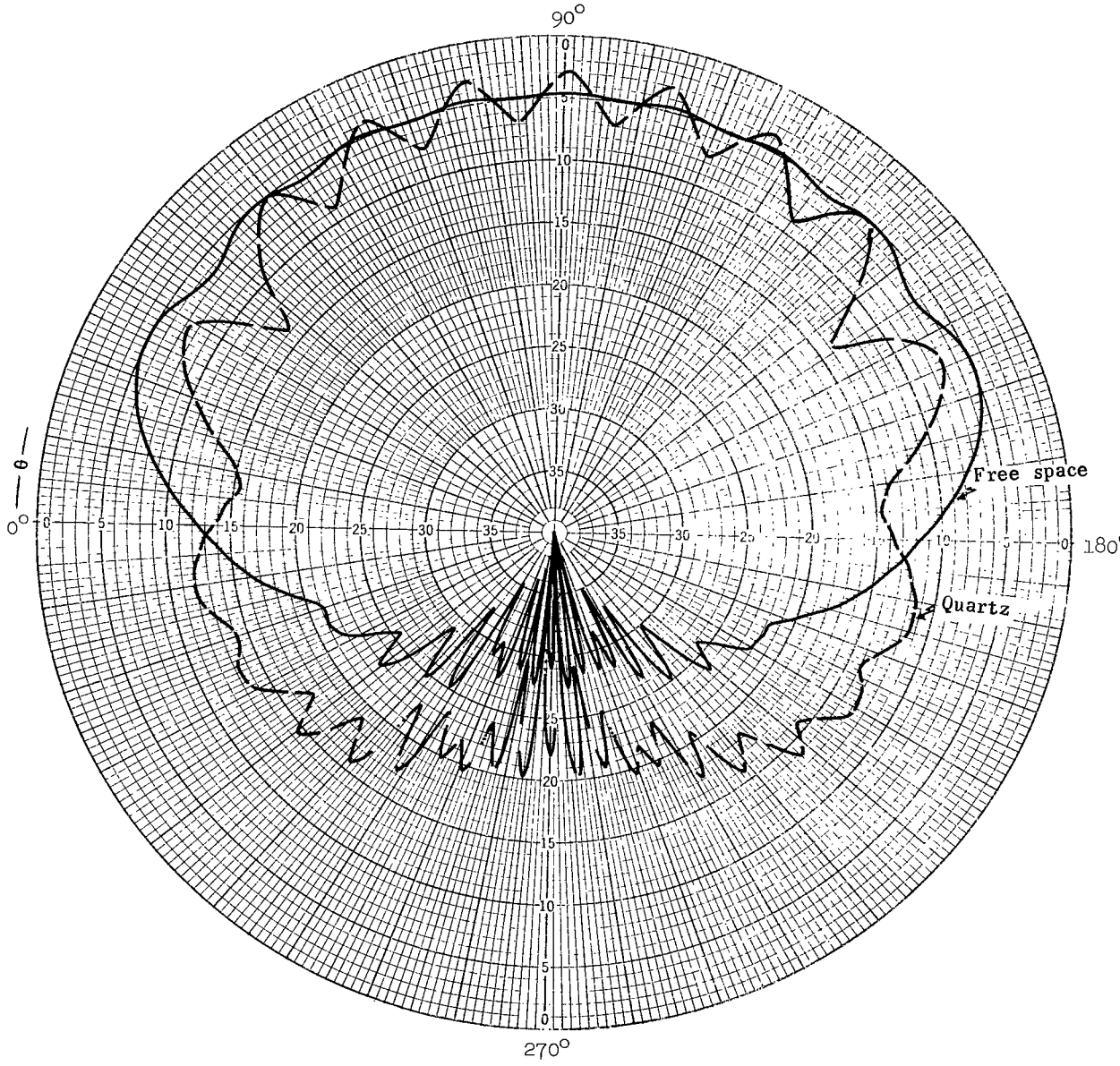

Figure 12.- E-plane radiation pattern at 9.0 GHz for H-plane horn radiating into free space and into 0.322-cm-thick quartz slab.

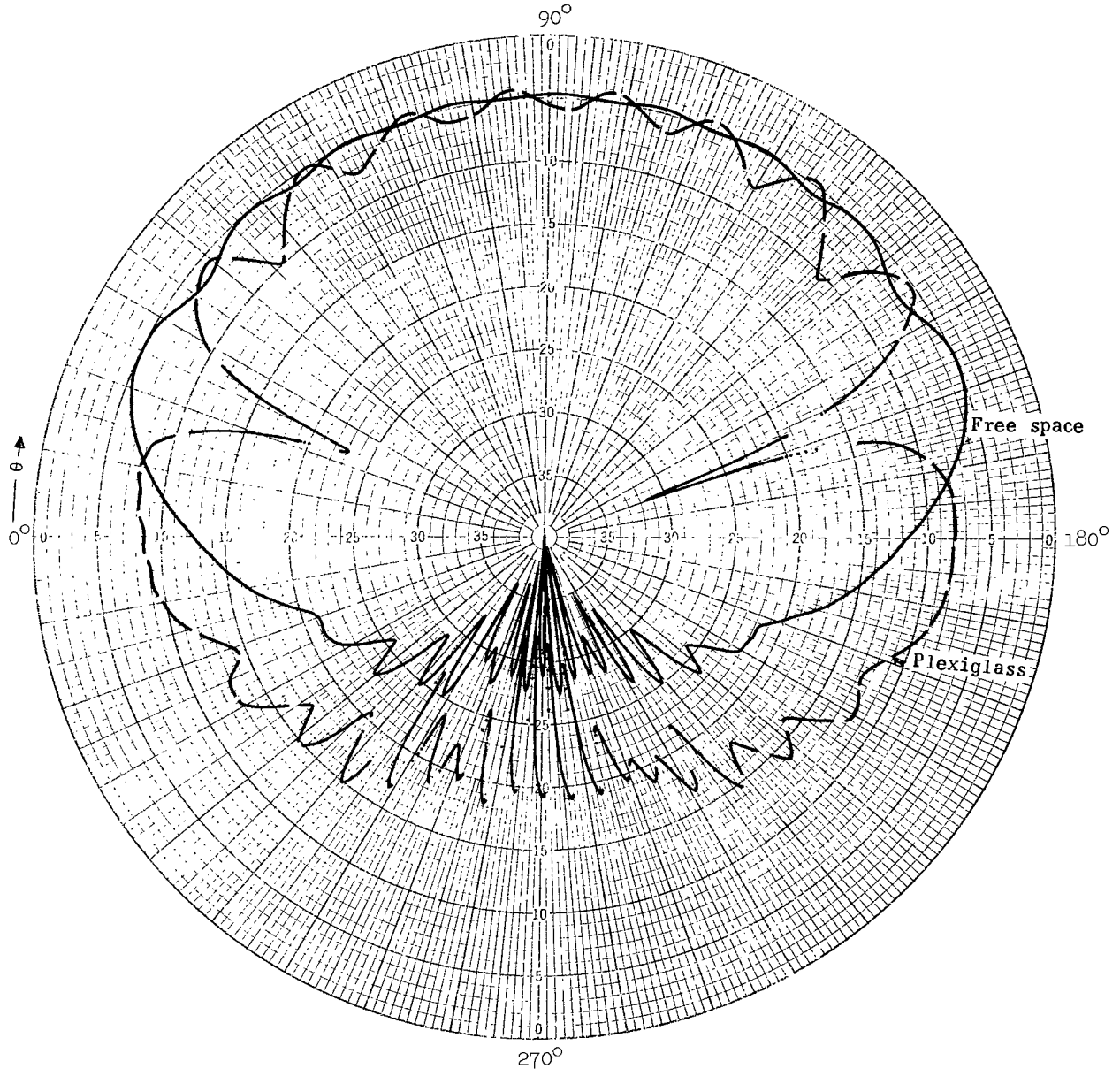

Figure 13.- E-plane radiation pattern at 9.0 GHz for H-plane horn radiating with free space and into 0.345-cm-thick plexiglass slab.

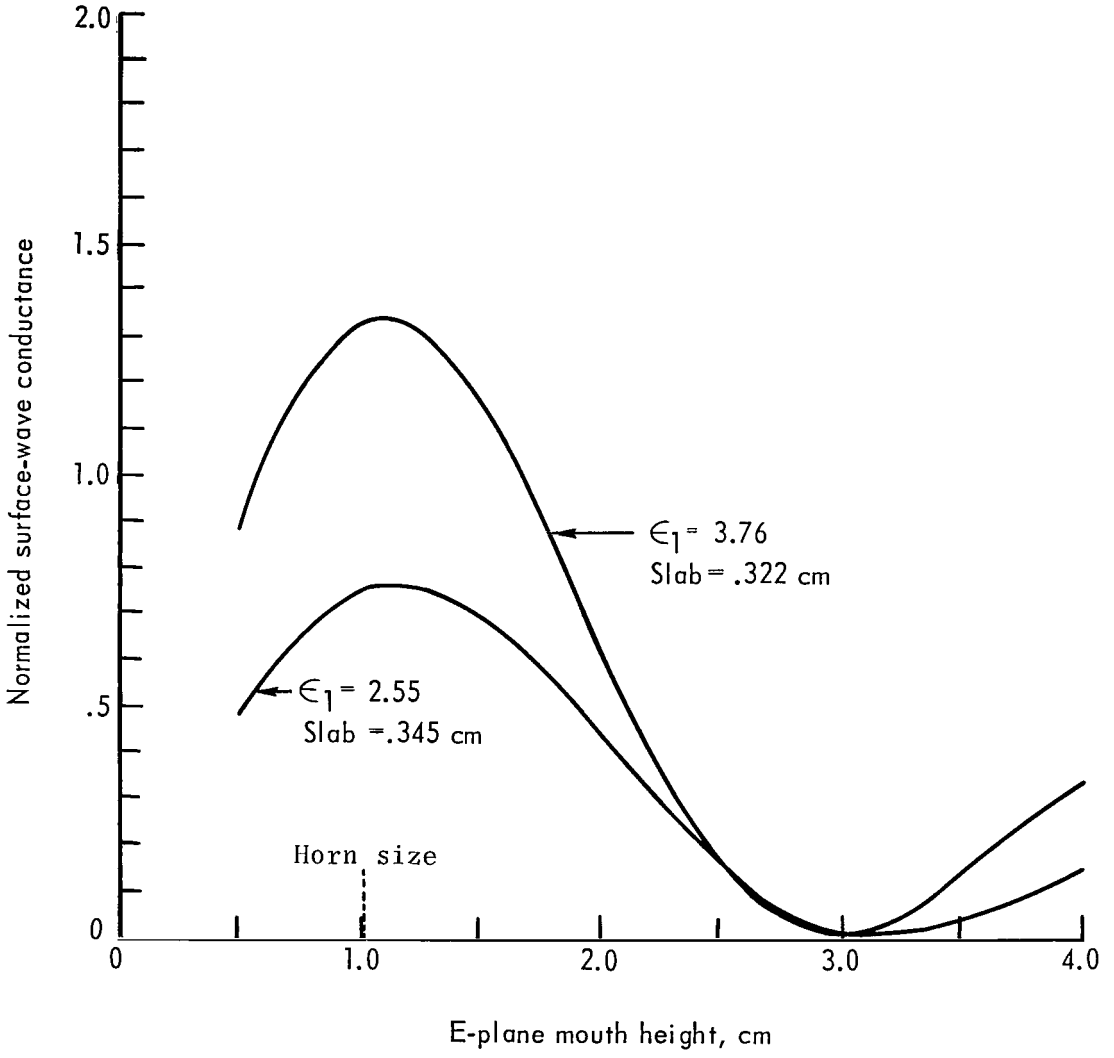

Figure 14.- Normalized surface-wave conductance at 9.0 GHz for H-plane horn as a function of E-plane mouth height. H-plane mouth width = 6.248 cm.

"The aeronautical and space activities of the United States shall be conducted so as to contribute . . . to the expansion of human knowledge of phenomena in the atmosphere and space. The Administration shall provide for the widest practicable and appropriate dissemination of information concerning its activities and the results thereof."

—NATIONAL AERONAUTICS AND SPACE ACT OF 1958

NASA SCIENTIFIC AND TECHNICAL PUBLICATIONS

TECHNICAL REPORTS: Scientific and technical information considered important, complete, and a lasting contribution to existing knowledge.

TECHNICAL NOTES: Information less broad in scope but nevertheless of importance as a contribution to existing knowledge.

TECHNICAL MEMORANDUMS: Information receiving limited distribution because of preliminary data, security classification, or other reasons.

CONTRACTOR REPORTS: Scientific and technical information generated under a NASA contract or grant and considered an important contribution to existing knowledge.

TECHNICAL TRANSLATIONS: Information published in a foreign language considered to merit NASA distribution in English.

SPECIAL PUBLICATIONS: Information derived from or of value to NASA activities. Publications include conference proceedings, monographs, data compilations, handbooks, sourcebooks, and special bibliographies.

TECHNOLOGY UTILIZATION PUBLICATIONS: Information on technology used by NASA that may be of particular interest in commercial and other non-aerospace applications. Publications include Tech Briefs, Technology Utilization Reports and Notes, and Technology Surveys.

Details on the availability of these publications may be obtained from:

SCIENTIFIC AND TECHNICAL INFORMATION DIVISION

NATIONAL AERONAUTICS AND SPACE ADMINISTRATION

Washington, D.C. 20546